DOE/ET-53088-259 IFSR #259

The Effects of Sloshing Energetic Particles on Ballooning Modes in Tokamaks

D. P. Stotler[a] and *H. L. Berk*

Institute for Fusion Studies
The University of Texas at Austin
Austin, Texas 78712

October 1986

[a] Present Address: Princeton Plasma Physics Laboratory,
Princeton, New Jersey.

The Effects of Sloshing Energetic Particles on Ballooning Modes in Tokamaks

D. P. Stotler[a] and *H. L. Berk*

Institute for Fusion Studies

The University of Texas at Austin

Austin, Texas 78712

Abstract

Distributions that give rise to energetic trapped particle pressures peaked in the "good curvature" region of a tokamak (sloshing distributions) are examined in an attempt to find stable regimes for both the magnetohydrodynamic (MHD) and precessional modes. It is the precessional drift destabilization of ballooning modes that inhibits bridging the unstable gap to second stability by the use of deeply-trapped energetic particles unless the hot particles have an extremely large energy (~ 0.35 MeV for a tokamak like PDX). Unfortunately, our calculations indicate that the sloshing particles do not have a significant stabilizing effect. An analytic treatment shows that complete stability can be found only if the sign of the energetic particle magnetic drift-frequency can be reversed from its value in vacuum bad curvature without hot species diamagnetism. This is difficult to do in a tokamak because of the destabilizing contribution of the geodesic curvature to the drift frequency. Furthermore, for each of the two sloshing distributions employed (one contains only trapped particles; the other includes trapped and passing particles), a new "continuum instability" (where asymptotically along the field line the mode is a propagating plane wave) is found to be driven by geodesic curvature. These results indicate that energetic sloshing particles are not able to bridge the unstable gap to second stability.

[a] Present Address: Princeton Plasma Physics Laboratory, Princeton, New Jersey.

I. Introduction

Recently, there has been a great deal of interest in the interactions between energetic particles and MHD ballooning modes in tokamaks.[1-5] It has long been known that a highly energetic hot electron ring population can provide stability for the magnetohydrodynamic (MHD) interchange mode in the Elmo Bumpy Torus[6-8] (EBT) device. The mechanism used relies on the fact that the ring electrons drift across field lines so rapidly that they do not respond to the usual MHD displacements and are therefore able to form a stabilizing diamagnetic well. A similar scheme was proposed for the tokamak geometry to allow access to the second stability[3,9] region in which ballooning modes are predicted to be stable. However, the introduction of a new species into the plasma brings with it an additional source of instability.[10,11] This effect was first identified in tokamaks in connection with perpendicular neutral beam injection experiments on PDX.[12] The so-called "fishbone" oscillations were observed to have a real frequency comparable to the drift frequency of the energetic particles, and were later explained theoretically as a trapped particle induced destabilization of the internal kink mode.[13] Subsequently, it was shown that a similar effect arises when the energetic particles interact with ballooning modes,[1,4,5,14] and that the resultant instability was a good candidate for the high-frequency "precursor" oscillations also observed in the PDX experiments.[14,15] It is apparent from these investigations that this new high-frequency ($\omega \sim \omega_{dh}$, the energetic particle precessional drift-frequency) branch could destroy the "path" to second stability created by energetic particle stabilization of the low-frequency ($\omega \ll \omega_{dh}$) MHD branch.

A modification to the above scheme involves establishing "sloshing ions"; that is, energetic trapped particles with turning points in the good curvature region of the tokamak so that $\omega_{*h} \cdot \omega_{dh} < 0$ (ω_{*h} is the energetic particle diamagnetic drift-frequency). Although they would be more difficult to introduce and maintain in the machine, they are not expected to be susceptible to resonant particle destabilization.[3] In this paper we investigate their effects in more detail using both numerical and analytical techniques. We will consider the bounce frequency of the energetic species to be larger than ω and ω_{dh}.

Numerically, it is found that there is little reduction in the growth rate of the high-frequency instability obtained by placing a larger percentage of the trapped particle turning

points in the good curvature region. It is apparent that to do as well as a deeply-trapped distribution with the same midplane pressure gradient requires such a narrow pitch angle distribution that the condition $\tau = 1 + \frac{1}{B}\frac{\partial P_\perp}{\partial B} < 0$ ($P_\perp$ is the perpendicular component of the pressure, a function of the magnetic field strength B) is likely; $\tau < 0$ leads to a mirror-mode instability.[16,17]

In addition, the presence of a continuum instability is predicted by an examination of the ballooning mode equation in the limit that the radial wavenumber is much larger than the poloidal wavenumber. These modes are of interest when parameters are such that outgoing waves along the field line amplify in space. One then finds unstable purely propagating waves at infinity. When the energetic species is completely trapped, the restrictions imposed on the distribution to keep $\tau > 0$ imply that there is still a significant number of resonant particles ($\omega_{*h} \cdot \omega_{dh} > 0$) present in the system. The negative dissipation provided by these particles destabilizes the positive energy shear Alfvén waves ($\omega = \omega_A$; ω_A is the Alfvén frequency) arising from the field-line bending and inertia terms in the ballooning mode equation. A distribution containing circulating as well as trapped particles has also been examined. In this case we can increase the percentage of trapped particles having turning points on the inside of the tokamak and still maintain $\tau > 0$. Then, the continuum instability driven by the negative dissipation is removed, but another branch of the continuum solutions is predicted to be unstable (quite surprisingly) as a result of the presence of a large pressure peak in the good curvature region.

An analytic treatment indicates that the sloshing energetic particle distribution is, if anything, more unstable than a deeply-trapped distribution. The primary effect of achieving drift reversal ($\omega_{*h} \cdot \omega_{dh} < 0$) via energetic particle diamagnetism is to remove the negative dissipation arising from the energetic particle drift resonance. It is this dissipation that stabilizes the precessional mode for small values of the hot pressure gradient when a deeply-trapped distribution is used. The stabilizing effect of the sloshing particles appears only if $\omega_* \cdot \omega_{dh} < 0$ where the energetic particle diamagnetic contribution to the hot particle drift is excluded in evaluating ω_{dh}. In a tokamak, this is difficult to achieve because of the destabilizing contribution of the geodesic curvature. These various results lead us to conclude that energetic particles with a sloshing ion distribution are ineffective in bridging

the unstable gap to second stability and that deeply-trapped particles of the same energy would have a greater stabilizing influence.

The rest of this paper is organized as follows. In Sec. II we present the basic equations and describe our numerical model; Sec. III discusses the results of the numerical computations for localized eigenmodes, while Sec. IV focuses on the continuum instabilities. In Sec. V we describe a simple analysis of the eigenmode equations given in Sec. III. Finally, in Sec. VI we summarize our results and draw some conclusions.

II. Basic Equations and Numerical Model

The equations we will solve here treat the background, or core, plasma in the usual MHD fashion. The energetic particles are assumed to have high-bounce-frequency ($\omega \ll \omega_b$, the bounce frequency), but we allow for modes with $\omega \sim \omega_{dh}$. Several authors have derived equations describing such a system in the high-mode-number limit;[10,17,18] from their results, we obtain

$$\begin{aligned} &\mathbf{B}\cdot\nabla\left[\frac{\sigma|\nabla S|^2}{B^2}(\mathbf{B}\cdot\nabla\varphi)\right]+\varphi B\hat{e}\cdot\boldsymbol{\kappa}\left(Q_L-\frac{\sigma}{\tau}\varphi B\hat{e}\cdot\boldsymbol{\kappa}\right) \\ &\quad+\varphi\hat{e}\cdot\boldsymbol{\kappa}\left(\frac{\sigma}{\tau}\hat{e}\cdot\hat{\nabla}P_\perp+\hat{e}\cdot\hat{\nabla}P_\parallel\right)+\omega\left(\omega-\omega_{*i}\right)\frac{|\nabla S|^2\varphi}{V_A^2}=0, \end{aligned} \tag{1a}$$

and

$$\tau\left(Q_L-\frac{\sigma}{\tau}\varphi B\hat{e}\cdot\boldsymbol{\kappa}\right)=m_h\int d^3v\frac{\omega-\omega_*}{\omega-\langle\omega_d\rangle}\mu^2\frac{\partial F_h}{\partial E}\langle Q_L\rangle\,, \tag{1b}$$

$$P_\perp=\sum_j\frac{m_j}{2}\int d^3v v_\perp^2F_j,$$

$$P_\parallel=\sum_j m_j\int d^3v v_\parallel^2F_j.$$

Here, φ represents the perturbed electrostatic potential, and Q_L, the perturbed magnetic field parallel to the equilibrium field, $\mathbf{B}=\hat{b}B$, as observed in a Lagrangian frame. Other quantities appearing in Eqs. (1a) and (1b) are $\sigma=1+\left(P_\perp-P_\parallel\right)/B^2$, $\tau=1+\frac{1}{B}\frac{\partial P_\perp}{\partial B}$, $\boldsymbol{\kappa}=\hat{b}\cdot\nabla\hat{b}$, $P_\perp(P_\parallel)$ the perpendicular (parallel) pressure, $V_A^2=B^2/\rho$; ρ, the mass density; $\mu=\frac{v_\perp^2}{2B}$, $E=\frac{v_\parallel^2}{2}+\mu B$, $\hat{\nabla}=\nabla-(\nabla B)\frac{\partial}{\partial B}$, and m_h, the energetic particle mass. The three

drift frequencies needed are

$$\omega_{*i} = -\frac{B}{\rho}\sum_j \frac{\hat{e}\cdot\nabla P_{\perp j}}{\Omega_j},$$

$$\omega_* = \frac{B}{\Omega_h}\frac{\hat{e}\cdot\nabla F_h}{\partial F_h/\partial E},$$

and

$$\omega_d = -\frac{B}{\Omega_h}\mu\hat{e}\cdot\nabla B,$$

where Ω_j refers to the cyclotron frequency for the jth species with the subscript h being used to represent the energetic trapped particles. The magnitude of $B(\theta)$ is given by $B_0(1-\epsilon\cos\theta)$, with ϵ the inverse aspect ratio. The brackets in Eq. (1b) imply time averages along the bounce orbit, $\langle f(s)\rangle = \oint \frac{ds}{|v_\parallel|} f(s) / \oint \frac{ds}{|v_\parallel|}$, s being the distance along the field line. Finally, as is appropriate in the high-mode-number limit, the cross-field dependence of the perturbed quantities is represented by an eikonal term $\exp(iS)$ with $\hat{b}\cdot\nabla S = 0$, and $\hat{e} = \hat{b}\times\nabla S/B$. In obtaining Eq. (1a) from the result of Catto, Hastie, and Connor,[18] we have dropped the higher order finite Larmor radius terms (ω_g and ω_k in their work), but retained the lowest order contribution ω_{*i}. Due to the fact that the energetic particles are trapped in a rather shallow magnetic well, their parallel velocities and pressures are a factor of $\epsilon = r/R_0$ smaller than the corresponding perpendicular quantities (r = minor radius; R_0 = major radius). Since these effects appear in terms of order β_h (β = ratio of thermal to magnetic energy), we neglected them in writing Eqs. (1a) and (1b). For most of our numerical work, we will use a model trapped particle distribution function

$$F_h(E,\mu,\psi) = \begin{cases} \frac{8}{15}(2\pi)^{-3/2}\frac{B_c^{3/2}}{m_h v_h^7 C(0)}\hat{P}_{\perp h}\left[1-\frac{(\psi-\psi_0)^2}{\Delta\psi^2}\right]\frac{(\mu B_c - E)e^{-E/v_h^2}}{\left[1+\frac{\left(\frac{\mu B_c}{E}-1\right)^2}{\Delta\lambda^2}\right]}, & \frac{E}{B_c} < \mu < \frac{E}{B_{\min}}, \\ 0, & 0 < \mu < \frac{E}{B_c}. \end{cases} \tag{2}$$

The dependence of $P_{\perp h}$ on the poloidal angle θ can be expressed in terms of the integral

$$C(\theta) = B^{3/2}\int_1^{B_c/B} \frac{d\lambda\,\lambda}{\sqrt{\frac{B_c}{B}-\lambda}}\frac{(\lambda-1)}{\left[1+\frac{(\lambda-1)^2}{\Delta\lambda^2}\right]};$$

namely,

$$P_{\perp h}(\theta) = \hat{P}_{\perp h}\left[1 - \frac{(\psi-\psi_0)^2}{\Delta\psi^2}\right]\frac{C(\theta)}{C(0)} \equiv \hat{P}_{\perp h}\left[1 - \frac{(\psi-\psi_0)^2}{\Delta\psi^2}\right]p_\perp(\theta).$$

A similar expression for $P_{\parallel h}$ is found to be convenient (it is needed only in the equilibrium calculation),

$$P_{\parallel h}(\theta) = 2\hat{P}_{\perp h}\left[1 - \frac{(\psi-\psi_0)^2}{\Delta\psi^2}\right]\frac{r}{R_0}p_\parallel(\theta),$$

with

$$p_\perp(\theta) = -2\frac{r}{R_0}\left[\left(B\frac{d\theta}{dB}\right)\frac{dp_\parallel}{d\theta} - p_\parallel\right].$$

The pitch angle, $\lambda = \mu B_c/E$, varies from $\lambda = 1$ to $\lambda = B_c/B_{\min}$, where $B_c = B(\theta = \theta_0)$ and $B_{\min} = B(\theta = 0)$; θ_0 represents the largest turning point for the trapped particles. Particles having $\lambda \lesssim B_c/B_{\min}$ are trapped near $\theta = 0$ in the "bad curvature" region of the tokamak, while those with $\lambda = 1$ travel between $-\theta_0$ and $+\theta_0$.

We will also consider a second distribution that contains passing as well as trapped energetic particles; namely,

$$F_h(E,\mu,\psi) = \frac{8}{15}(2\pi)^{-3/2}\frac{B_c^{3/2}}{m_h v_h^7 C(0)}\hat{P}_{\perp h}\left[1 - \frac{(\psi-\psi_0)^2}{\Delta\psi^2}\right]\frac{E\exp\left(-\frac{E}{v_h^2}\right)}{\left[1 + \left(\mu B_c/E - 1\right)^2/\Delta\lambda^2\right]}, \tag{3}$$

where in this case

$$C(\theta) = B^{3/2}\int_0^{B_c/B}\frac{d\lambda\,\lambda}{\sqrt{\frac{B_c}{B} - \lambda}}\frac{1}{\left[1 + \frac{(\lambda-1)^2}{\Delta\lambda^2}\right]},$$

and $\theta_0 \equiv \pi$. Despite the change in the limits of the pitch angle integral defining $C(\theta)$, the magnetic moment integral in Eq. (1b) still ranges from E/B_c to E/B, including only the trapped particles. This is due to the fact that when the passing particles have a high transit frequency (analogous to the bounce frequency for trapped particles), they do not contribute to the kinetic term in Eq. (1b).[19] They do, however, enter the calculation through the fluid pressure gradient term in Eq. (1a) as well as appear in the various equilibrium quantities involving the energetic species pressure.

The parameter $\Delta\lambda$ in Eqs. (2) and (3) can be varied to shift the emphasis of the distribution from $\lambda \cong B_c/B_{\min}$ ($\Delta\lambda \gg 1$; we will refer to this as the deeply-trapped case)

to $\lambda = 1$ ($\Delta\lambda \ll 1$, a sloshing distribution). When $\theta_0 \leq \pi$ and $\Delta\lambda \ll 1$, we are placing the turning points of most of the particles in the good curvature region so that $\omega_* \langle\omega_d\rangle < 0$ in an attempt to remove the resonant instability.

An analytic equilibrium can be obtained for a large aspect ratio, low β plasma having a sharp, localized, radial pressure gradient; the flux surfaces in this case are shifted circles. Solving the anisotropic equilibrium equation in the same manner as Rosenbluth et al.,[3] we obtain an expression for the eikonal $\nabla S = nq/r\left[\hat{\theta} + \hat{r}h(\theta)\right]$ (n = toroidal mode number), where $h(\theta) = S(\theta - \theta_k) - \alpha_c(\sin\theta - \sin\theta_k) - \alpha_h\left[g(\theta) - g(\theta_k)\right]$, $q = \frac{rB_T}{R_0 B_p}$ (B_p = poloidal component of the magnetic field), $S = \frac{r}{q}\frac{\partial q}{\partial r}$, $\alpha_c = -2R_0 q^2 \frac{dP_c}{dr}/B_0^2$, $\alpha_h = -2R_0 q^2 \hat{P}_{\perp h}\frac{\partial}{\partial r}\left[1 - \frac{(\psi(r)-\psi_0)^2}{\Delta\psi^2}\right]\Big/ B_0^2$

$$g(\theta) = \begin{cases} p(\tilde{\theta}) - \frac{\tilde{\theta}}{\pi}p(\theta_0), & 0 < \tilde{\theta} < \theta_0 \\ \left(1 - \frac{\tilde{\theta}}{\pi}\right)p(\theta_0); & \theta_0 < \tilde{\theta} < 2\pi - \theta_0 \\ \left(\frac{2\pi - \tilde{\theta}}{\pi}\right)p(\theta_0) - p(2\pi - \tilde{\theta}), & 2\pi - \theta_0 < \tilde{\theta} < 2\pi, \end{cases}$$

and $p(\theta) = \int_0^\theta d\theta' p_\parallel(\theta')$; θ is now the extended poloidal coordinate appearing in the ballooning mode representation, and $\tilde{\theta} = \theta \bmod 2\pi$. θ_k is the radial wavenumber; we will assume $\theta_k = 0$ for simplicity.

Now, if we redefine the perturbed field quantities

$$\delta Q \equiv \left(Q_L - \frac{\sigma}{\tau}\varphi B\hat{e}\cdot\boldsymbol{\kappa}\right) qrR_0,$$
$$\Phi \equiv \left(1 + h^2\right)^{1/2}\varphi,$$

Eqs. (1a) and (1b) become

$$\sigma\frac{\partial^2\Phi}{\partial\theta^2} - \frac{\sigma\Phi}{(1+h^2)}\left[\frac{(dh/d\theta)^2}{(1+h^2)} + h\frac{d^2h}{d\theta^2}\right] + \left(\frac{\partial\Phi}{\partial\theta} - \frac{h\frac{dh}{d\theta}\Phi}{1+h^2}\right)\frac{\partial\sigma}{\partial\theta}$$
$$+ \frac{\Phi}{(1+h^2)}D(\theta)\left\{\frac{\alpha_c}{2}\left(1 + \frac{\sigma}{\tau}\right) + \frac{\alpha_h}{2}\frac{\sigma}{\tau}p_\perp(\theta)\right\} \qquad (4a)$$
$$+ \frac{q^2R_0^2}{V_A^2}\omega\left(\omega - \omega_{*i}\right)\Phi = -\frac{\sigma D(\theta)}{(1+h^2)^{1/2}}\delta Q,$$

and

$$\tau\delta Q = m_h\int d^3v\frac{\omega - \omega_*}{\omega - \langle\omega_d\rangle}\mu^2\frac{\partial F_h}{\partial E}\left[\langle\delta Q\rangle + q^2\left\langle\frac{\sigma}{\tau}\frac{D(\theta)\Phi}{(1+h^2)^{1/2}}\right\rangle\right], \qquad (4b)$$

with $D(\theta) = \cos\theta + h(\theta)\sin\theta$. Two other input parameters are needed to specify the magnitudes of ω_{*i} and ω_d. We write

$$\omega_{*i} = -\omega_{*0}\left(\alpha_c \frac{T_i}{T_i+T_e} + \frac{Z_i}{Z_h}\frac{m_h}{m_i}\left\{\frac{(1-\tau)}{\tau}\left[\alpha_c - 2\sigma q^2 D(\theta)\right] + \frac{\alpha_h p_\perp(\theta)}{\tau}\right\}\right), \quad (5a)$$

$$\omega_d = -\lambda\frac{E}{v_h^2}\omega_{d0}\left[\frac{\sigma}{\tau}D(\theta) - \frac{\alpha_c}{2q^2\tau} - \frac{\alpha_h}{2q^2}\frac{p_\perp(\theta)}{\tau}\right], \quad (5b)$$

where T_i and T_e are ion and electron temperatures, $\omega_{*0} = \frac{nV_A^2}{2r\Omega_i q R_0}$, $\omega_{d0} = \frac{nqv_h^2}{rR_0\Omega_h}$; ω_{d0}/ω_A (this quantity is proportional to the product of mode number and energetic particle temperature), and ω_{*0}/ω_{d0} (at constant α_c this quantity is related to the temperature ratio, T_i/T_h) are input parameters. $\omega_A = \frac{V_A}{qR_0}$ is the Alfvén frequency, and Z_j is the atomic number of species j.

In order to calculate $\hat{P}_{\perp h}$ from α_h, we need to know ψ and $\Delta\psi$. We set $\psi = \psi_0 + \frac{\Delta\psi}{2}$ so that we examine the system's response along a field line passing midway through the gradient region of radial width $\Delta_r = \Delta\psi/R_0B_p$; we use Δ_r/r as an input parameter.

The method of solution involves representing δQ in terms of a complete set of Fourier functions over the interval, $0 < \tilde{\theta} < \theta_0$; from Eq. (4b), we see that $\delta Q = 0$ outside of this interval and must be even about $\tilde{\theta} = 0$. Equations (4a) and (4b) are integrated numerically starting at some large value of θ, $\theta_m \gg 2\pi$. At this point Eqs. (4a) and (4b) have an approximate Floquet solution

$$\Phi(\theta) = \hat{\Phi}(\theta)e^{i\int k(\theta)d\theta},$$

with $\hat{\Phi}(\theta)$ having period 2π;[20] $k(\theta)$ is nearly constant over a period. If this local wavenumber is treated as a constant, $k(\theta) \cong k(\theta_m)$, its value can be determined numerically by integrating twice over a 2π region near θ_m with specified initial conditions.[21,22] In this procedure, two values for $k(\theta_m)$ are found; the one yielding $\mathrm{Re}\frac{\partial\omega}{\partial k} > 0$ (outgoing waves) is chosen. This choice is usually consistent with $\mathrm{Im}\, k > 0$ (spatially damped waves). Alternative approaches to the solution of Eqs. (4a) and (4b) are required when these two criteria are not met simultaneously; one such method will be described in Sec. IV. A rigorous discussion of how to choose the boundary conditions is given in Ref. 22.

Once $k(\theta_m)$ is determined, it is used to establish the boundary condition $\frac{1}{\Phi}\frac{d\Phi}{d\theta}(\theta_m)$. This is then matched to the large θ solution of the full integro-differential equation; the

resulting eigenvalues are verified as being insensitive to θ_m. We assume even eigenmodes centered about the origin (i.e., $\theta_k = 0$). A shooting method is employed to vary the eigenfrequency ω until a zero slope at the origin is found.

In the process of specifying a narrow peak in $P_{\perp h}(\theta)$ near θ_0, one necessarily incurs significant pressure gradients along the field line since $P_{\perp h}(\theta)$ must vanish at θ_0 for a purely trapped distribution. As a consequence, $\left|\frac{1}{B}\frac{\partial P_{\perp h}}{\partial B}\right|$ may be large. It is well known that if $\tau \leq 0$, the plasma will be mirror-mode unstable.[16,17,23] Also, the expression for ω_d in Eq. (5b) becomes invalid if $\tau = 0$ somewhere.

Requiring $\tau > 0$ places restrictions on $\Delta\lambda$, α_h, and Δ_r/r. It can be shown for the distribution given in Eq. (2) that the "largest" negative value of $\frac{1}{B}\frac{\partial P_{\perp h}}{\partial B}$ is

$$\frac{1}{B}\frac{\partial P_{\perp h}}{\partial B}\Big|_{\max} \simeq -0.33 \ .$$

To obtain

$$\frac{1}{B}\frac{\partial P_{\perp h}}{\partial B}\Big|_{\max} \simeq -1,$$

we need only $\Delta\lambda \lesssim 0.01$ for these parameters. Thus, it appears that we are quite limited in the values of $\Delta\lambda$ that we can use.

Note also that these problems can be formally circumvented by setting $\Delta_r/r = 0$ so that $\sigma = \tau = 1$. This represents the limit of zero plasma pressure with finite pressure gradient. Such an assumption is convenient as it greatly simplifies Eqs. (4a) and (4b); however, it is also physically unrealistic. For this reason, we will keep in mind the restrictions necessary to maintain $\tau > 0$ in an actual experiment, even if we set $\Delta_r/r = 0$ in our calculation.

However, when we employ a distribution containing both circulating and trapped energetic particles such as Eq. (3), $P_{\perp h}$ does not vanish anywhere along the field line. Thus, the pressure can be highly peaked in the good curvature region without incurring large negative values of $\frac{1}{B}\frac{\partial P_{\perp h}}{\partial B}$. This approach is more realistic than the previous one if we consider the circulating, or passing, component to consist of trapped particles that have undergone pitch angle scattering.

For convenience, we have chosen the peak of the pitch angle distribution to be at $\lambda = 1$; it turns out that $\frac{1}{B}\frac{\partial P_{\perp h}}{\partial B} < 0$ near $\theta = \pi$ in this case. However, by shifting

the peak to a slightly smaller value, say $\lambda \cong 1 - \Delta\lambda$ (increase the fraction of passing particles), this effect may be removed completely so that $\frac{1}{B}\frac{\partial P_{\perp h}}{\partial B} > 0$ all along the field line. In other words, the problems with τ vanishing can be eliminated by altering the details of the distribution, whereas the sharp drop in $P_{\perp h}(B)$ is a fundamental feature of the purely-trapped distribution. By using the one in Eq. (3), we can achieve a considerable level of anisotropy and, hence, place the turning points of most of the trapped particles near $\theta = \pi$ (i.e., $\mu = E/B_c$). Consequently, we can increase the contribution of particles with $\omega_* \langle\omega_d\rangle < 0$ to the kinetic integral in Eq. (4b) relative to what can be done using a distribution that contains only trapped particles.

III. Numerical Results

In Fig. 1, we plot the growth rate $\mathrm{Im}\frac{\omega}{\omega_A}$ found by integrating Eqs. (4a) and (4b) with the distribution Eq. (2) as a function of α_h. The parameters used here are $S = 0.6$, $\alpha_c = 0.8$, $r/R_0 = 0.2$, $q = 2$, $Z_i = Z_h$, and $m_i = m_h$; these choices were made to facilitate comparisons with similar theoretical work published previously.[1,4,5] We set $\sigma = \tau = 1$ for simplicity in generating Fig. 1. For more physically realistic cases, the restrictions on $\Delta\lambda$ and α_h outlined above should be adhered to. Calculating σ and τ properly leads to a slightly lower growth rate. However, when τ approaches zero, several numerical integration routines fail as a consequence of the inability to properly calculate ∇B.

Curves (i) and (ii) in Fig. 1 represent the result of using $\theta_0 \cong \pi/4$, $\Delta\lambda \gg 1$, with $\omega_{d0}/\omega_A = 0.636$. We set $\omega_{*0}/\omega_{d0} = 0$ for simplicity, denoting the limit $T_i/T_h \to 0$. This is essentially the standard deeply-trapped case investigated previously.[3,4] For small α_h, we see the stabilizing effect of the energetic particles on the low-frequency ($\mathrm{Re}\,\omega \ll \omega_d$), MHD root [curve (i)]. At larger α_h, as $\mathrm{Im}\,\frac{\omega}{\omega_A}$ vanishes for this branch, the high-frequency ($\mathrm{Re}\,\omega \sim \omega_d$), precessional branch [curve (ii)] becomes unstable. It was the desire of this investigation to remove the latter instability by altering the distribution of the energetic particles.

It is already known that increasing ω_{d0}/ω_A will move the critical α_h for the high-frequency branch to the right, opening a window in which both modes are stable.[1] We demonstrate this in the marginal stability plot shown in Fig. 2. The parameters used here

are the same as in curves (i) and (ii) of Fig. 1 except that α_h and ω_{d0}/ω_A are being varied so that $\mathrm{Im}\,\omega/\omega_A = 10^{-3}$ for each of the MHD (lower curve) and precessional (upper curve) branches. The resulting stable and unstable regions are labeled accordingly.

Since ω_{d0}/ω_A is proportional to n, the toroidal mode number, smaller values of ω_{d0}/ω_A can apply simply by specifying a lower n. There is a lower limit on n needed to retain the validity of the high-mode-number approximation used in deriving these equations (say, $n \sim 2-3$). If v_h^2 is large enough, this limit can prevent ω_{d0}/ω_A from being below 0.65, the critical value at which the window closes for this set of parameters. Using PDX-like parameters,[24] $n_i = 3\times 10^{13} cm^{-3}$, $B = 2$ Tesla, $q = 2$, $r = 25$ cm., we estimate $\omega_{d0}/\omega_A \cong 0.1n\left(\frac{m_h v_h^2}{100keV}\right)\left(\frac{2\mathrm{Tesla}}{B}\right)^2\left(\frac{3\times 10^{13} cm^{-3}}{n_i}\right)^{-1/2}\left(\frac{q^2}{4}\right)\left(\frac{25cm}{r}\right)$. To obtain $\omega_{d0}/\omega_A = 0.65$ with $n = 2$ and thereby provide a stable window of operation, we need $m_h v_h^2 = 325$keV, somewhat beyond present technology.

We should also mention that other instabilities may be present even if we are operating within this stable window. For instance, the discrete eigenmodes set up by the toroidal coupling of neighboring poloidal harmonics in the shear Alfvén spectrum[25] are destabilized by energetic particles.[21,26]

In curve (iii) of Fig. 1, we again consider $\omega_{*0}/\omega_{d0} = 0$, $\omega_{d0}/\omega_A = 0.636$, but now $\theta_0 = 3.04$ and $\Delta\lambda = 0.02$. Over the range shown, we note improved stability properties of the MHD branch relative to the deeply-trapped case for $\alpha_h > 0.7$. Examination of the real part of the frequency in this case shows that $\mathrm{Re}\,\omega \ll \omega_d$, so that we have yet to reach the point at which the MHD branch can be considered stable. Calculations for $\alpha_h \gtrsim 1.2$ [the intersection of curves (iii) and (iv) at this point is purely coincidental] in this case are prohibited by the failure of the eigenmode to satisfy the boundary conditions at infinity; namely, neither of the two possible k values correspond to both outgoing and spatially damped waves. This indicates that we need to consider continuum eigenmodes instead of the localized modes we have treated thus far. The procedure for doing this will be discussed shortly.

We now examine a case with $\omega_{*0}/\omega_{d0} = 1.10$ [curve (iv)] which has a reduced growth rate at $\alpha_h = 0$. For $\alpha_h \gtrsim 1$, the eigenfrequency has a significant real part ($\mathrm{Re}\,\omega \sim \omega_d$), as we would expect for the precessional mode. If the sloshing ion distribution is to be

effective, the growth rate of this mode should decrease as we place a larger percentage of the turning points near $\theta = \pi$. To test this hypothesis, we start with the point at $\alpha_h = 1.52$ on curve (iv), and reduce $\Delta\lambda$ at constant α_h to $\Delta\lambda = 0.013$; this leads to a decrease in Im $\frac{\omega}{\omega_A}$ to 0.155 . This represents a less than 10% reduction in growth rate from that found with $\Delta\lambda = 0.02$. Furthermore, at this point we should be concerned with τ going through zero. Amplifying outgoing wave boundary conditions again prevent us from extending curve (iv) further than shown in Fig. 1. These results indicate that the sloshing ion distribution in Eq. (2) is not strongly stabilizing. In Fig. 3, we present a plot of ReδQ as a function of θ for the point with $\alpha_h = 1.88$ on curve (iv) in Fig. 1. Clearly, the eigenfunction exhibits a large peak near $\theta = 0$, indicating an emphasis on the few resonant particles trapped in the bad curvature region. This appears to hinder stabilization of the high-frequency mode by sloshing particles.

IV. Continuum Eigenmodes

In those cases where the boundary condition at infinity is producing amplifying outgoing waves, we examine Eqs. (4a) and (4b) in the limit $\theta \to \infty$. This is equivalent to considering the radial wavenumber, $\vec{k}_\perp \cdot \hat{r}$, to be large relative to the poloidal wavenumber, $\vec{k}_\perp \cdot \hat{\theta}$, in the expression for $\vec{k}_\perp = \nabla S$. Asymptotically, the equations reduce to ones with constant coefficients, so that modes proportional to $e^{ik\theta}$ with k real are proper continuum eigenmodes. We search the real k spectrum for unstable roots and determine the k value that gives the maximum growth rate $\gamma_{\max}$. Close inspection of Eqs. (4a) and (4b) reveals that not only do the field-line bending and inertia terms remain as $\theta \to \infty$, but a piece of the kinetic term contributes as well. Namely, with $\sigma = \tau = 1$ and $\omega_{*i} = 0$,

$$\frac{d^2\Phi}{d\theta^2} + \frac{\omega^2}{\omega_A^2}\Phi = -\sin\theta\delta Q, \tag{6a}$$

$$\delta Q = -m_h \int d^3v \frac{\omega_*}{\omega - \langle\omega_d\rangle}\mu^2\frac{\partial F_h}{\partial E}\left[\langle\delta Q\rangle + \left\langle\Phi q^2 \sin\theta\right\rangle\right]. \tag{6b}$$

Physically, we have positive energy shear Alfvén plane waves at infinity, $\omega = \omega_A$. These are readily destabilized by the negative dissipation arising out of the drift resonance in Eq. (6b). A solution satisfying the pinch-point conditions[27]

$$D(k,\omega) = 0 \qquad \text{and} \qquad \frac{\partial D}{\partial k}(k,\omega) = 0,$$

where $D(k,\omega)$ is the effective dispersion relation for the system, occurs at $k = 0$ (purely periodic solutions). From Eqs. (6) one can show that $\omega(k) = \omega(-k)$ and $\omega(k+1) = \omega(k)$; hence near $k = 0$, we must have $\partial D/\partial k = 0$, or $D(k,\omega) = ak^2 - (\omega - \omega_0)$, where a and ω_0 are constants. Similarly, one can show that $\partial D/\partial k = 0$ at $2k =$ integer. Numerically, it is found that $\mathrm{Im}\,\omega_0 > 0$ and $\mathrm{Im}\,a < 0$ so that the local maximum in the growth rate for real k is at $k = 0$. Numerical searches over the whole range of k indicate that $k = 0$ is an absolute maximum as well; hence, $\gamma_{\max} = \mathrm{Im}\,\omega_0$.

As long as $\gamma_{\max} > 0$, an unstable eigenmode can be found for the system, although not necessarily of the type we have been seeking in the calculations leading to Fig. 1. If ω_e, the frequency of the localized eigenmode, lies between the contour mapped out in the upper half of the complex ω plane by all solutions of $D(\omega,k) = 0$ with k real and the real ω axis, spatial growth in the direction of the group velocity is the required boundary condition. In all other cases, the waves should be damped in the direction of the group velocity. This is insured if we can find the parameters determining the equilibrium such that $\gamma_{\max} \simeq 0$. Thus, an unstable eigenmode will have $\mathrm{Im}\,\omega_e > \mathrm{Im}\,\omega(k)$ for all real k, and we can return to solving the eigenmode equations, Eqs. (4a) and (4b), in the manner described in Sec. II.

We calculated $\gamma_{\max}$ as a function of $\Delta\lambda$ for the parameters used in curve (iii) of Fig. 1 at $\alpha_h = 1.5$ and found that $\gamma_{\max}$ decreased with $\Delta\lambda$, but to reach the point where $\gamma_{\max} \sim \mathrm{Im}\frac{\omega}{\omega_A}\,(\alpha_h = 0)\,/10$, we needed $\Delta\lambda = 2 \times 10^{-4}$ with $\sigma = \tau = 1$ [curve (i) in Fig. 4]. The fact that this represents a peak in $P_{\perp h}$ some two orders of magnitude narrower than allowed by $\tau > 0$ for physically reasonable values of Δ_r/r indicates that using other slightly different distributions will not improve the situation significantly. The stabilization arises from an overall increase in the number of particles with $\omega_*\,\langle\omega_d\rangle < 0$. These particles are nonresonant and give no contribution to the negative dissipation term. However, some particles are trapped in the bad curvature region and will always cause resonant destabilization so that $\gamma_{\max} > 0$ regardless of the value of $\Delta\lambda$.

Now we consider the distribution containing both trapped and circulating energetic particles, Eq. (3). The results of calculating $\gamma_{\max}$ (for the $k = 0$ continuum mode) with this distribution are shown in curve (ii) of Fig. 4; all parameters are as in curve (i). For

$\Delta\lambda = 0.02$, $\gamma_{\max}$ is significantly smaller than the growth rates predicted in curves (iii) and (iv) of Fig. 1. Thus, in solving Eqs. (4a) and (4b), we expect that the continuum instability will not interfere with the large θ boundary conditions. The fact that we have essentially stabilized this continuum mode would seem to indicate that the dominant contribution to the kinetic integral is from particles with $\omega_* \langle\omega_d\rangle < 0$, as we had hoped to achieve at the outset.

When we repeat the calculations leading to curve (iii) of Fig. 1 with the circulating-trapped distribution replacing the one in Eq. (2), we find qualitatively the same results as shown in curves (iii) and (iv) of Fig. 1 for $\alpha_h < 1.6$. That is, we do not find a marginally stable point for the localized eigenmode. However, calculations for $\alpha_h > 1.6$ lead again to unsatisfactory boundary conditions at infinity. Further investigation of the continuum limit given by Eqs. (6a) and (6b) in this case indicates that while the branch of solutions with $\gamma_{\max}$ occurring at $k = 0$ may be nearly stable, another branch with the growth rate for real k peaking at $k = 1/2$ (solutions have period 4π) is clearly unstable. This root also satisfies the pinch-point conditions. Whereas the mode frequencies at $k = 0$ had significant real parts indicative of a wave-precessional drift resonance, the ones calculated at $k = 1/2$ are almost purely imaginary with $\gamma_{\max}$ on the order of MHD growth rates.

This instability is due to the presence of a large energetic particle pressure peak in the good curvature region. Normally, one would think of this as aiding stability via the fluid pressure gradient-curvature terms on the left-hand side of Eq. (1a). The large pressure peak and low mode frequency allow us to assume that $\left|\omega / \langle\omega_d\rangle\right| \ll 1$, at least for the dominant part of the pitch angle distribution. In this case, we obtain a result familiar from EBT theory. Namely, the energetic particles produce through the kinetic term a contribution similar in magnitude but opposite in sign to the fluid pressure gradient-curvature terms (i.e., the energetic particles dig a diamagnetic well; see, for example, Ref. 28 and references therein). In situations involving average good curvature, the stabilizing fluid terms dominate so that the ballooning instability does not arise. In Eqs. (6a) and (6b), however, the fluid terms do not appear since they are smaller than the field-line bending and inertia terms by a factor of $1/S\theta$. The kinetic contribution, destabilizing in good curvature and represented by δQ on the right-hand side of Eq. (6a), is then uncancelled except for a

small amount of field-line bending entering through the $d^2\Phi/d\theta^2$ term. That δQ has a sign consistent with instability can be seen if we look at Eq. (6b) under the assumptions that $\omega \ll \langle\omega_d\rangle$, $\langle\delta Q\rangle < \langle\Phi q^2 \sin\theta\rangle$, and note that $\omega_* \frac{\partial F_h}{\partial E} / \langle\omega_d\rangle > 0$ in good curvature. Since this kinetic term is comparable in magnitude to the fluid MHD instability drive terms, we expect the resultant instability to have $\gamma_{\max}$ on the order of MHD growth rates. We will examine this mode in a more quantitative manner in Sec. V.

While it appears that there should be a stability threshold for this mode if α_h is small enough (because of the stabilizing influence of the field-line bending term), numerical calculations indicate a nonzero growth rate for $\alpha_h > 0$, as shown in curve (i) of Fig. 5. For large α_h, the mode frequency is largely imaginary, but becomes mostly real for small α_h ($\alpha_h \lesssim 0.7$ in this case), as can be seen in curve (ii) of Fig. 5. When α_h is lowered, the mode becomes less like a fluid MHD instability driven by the energetic particles and more like an Alfvén wave that is destabilized by the negative dissipation of the energetic particles. The transition should occur when the real and imaginary parts of Eq. (6b) are comparable.

From these results, we can conclude that if $\omega_* \langle\omega_d\rangle > 0$ on average, the continuum instability with growth rate peaking at $k = 0$ will be present, whereas if $\omega_* \langle\omega_d\rangle < 0$, the one at $k = 1/2$ appears. We should emphasize that a sloshing distribution (so that $\langle\Phi \sin\theta\rangle$ is not small) and high-bounce-frequency ordering (so that δQ enters Eq. (6a) at the same order as the other two terms) are necessary for these modes to be unstable.

V. Analytic Results

We now examine Eqs. (4a) and (4b) analytically and attempt to understand the conditions for stabilizing the precessional mode and the $k = 1/2$ continuum instability. For simplicity, we set $\Delta_r/r = 0$ so that $\sigma = \tau = 1$, and assume $\omega_{*i} = 0$. To do the pitch angle integral in Eq. (4b), we assume that all of the averages can be evaluated at some representative pitch angle for the distribution λ_*. For example, if all of the particles are deeply trapped, we set $\lambda_* \lesssim B_c/B_{\min}$; this amounts to evaluating the averaged quantity at $\theta = 0$, which approaches an exact result as $\theta_0 \to 0$. On the other hand, for a purely sloshing distribution, we would use $\lambda_* \simeq 1$. The rest of the velocity integrations can be done exactly using the distribution specified in Eq. (2).

Solving for δQ in this manner, we obtain

$$\delta Q = \frac{-\left\langle \Phi D(\theta)/\left(1+h^2\right)^{1/2}\right\rangle_* \frac{\alpha_h}{2} p_\perp(\theta) H(a)}{\langle D(\theta)\rangle_* - \frac{\alpha_c}{2q^2} - \frac{\alpha_h}{2q^2}\langle p_\perp(\theta)\rangle_* [1-H(a)]}. \tag{7}$$

The angle brackets with $*$ subscript indicate a bounce average along the field line, as before, but evaluated at the specified pitch angle λ_*. We will retain this convention for the rest of this sub-section. Also, $H(a)$ arises from doing the energy integral, and is given by[29]

$$H(a) = 1 + \frac{2}{5}a + \frac{4}{15}a^2 + \frac{8}{15}a^3 + \frac{8}{15}a^{7/2} Z\left(a^{1/2}\right), \tag{8}$$

with

$$a = -\frac{\omega}{\omega_{d0}} \left\langle \lambda \left[D(\theta) - \frac{\alpha_c}{2q^2} - \frac{\alpha_h}{2q^2} p_\perp(\theta) \right] \right\rangle_*^{-1}.$$

Z is the plasma dispersion function defined by

$$Z(\zeta) = \frac{1}{\sqrt{\pi}} \int_{-\infty}^{\infty} dx \frac{e^{-x^2}}{x - \zeta}$$

for $\mathrm{Im}\,\zeta > 0$ and by its analytic continuation for $\mathrm{Im}\,\zeta \leq 0$.[30]

Note that the only field line dependence in Eq. (7) is $p_\perp(\theta)$. It is quite apparent, however, from Fig. 3 that the actual eigenfunction can differ significantly from the double-humped form we expect to see for $p_\perp(\theta)$ with $\Delta\lambda = 0.02$. This discrepancy points out one

of the problems with this simplified analysis; nonetheless, we hope to be able to achieve here a qualitative understanding of the precessional mode.

We now substitute Eq. (7) for δQ into Eq. (4), and rearrange terms to obtain

$$\frac{d^2\Phi}{d\theta^2} - \frac{\Phi}{(1+h^2)}\left[\frac{(dh/d\theta)^2}{(1+h^2)} + h\frac{d^2h}{d\theta^2}\right] + \frac{\Phi D(\theta)}{(1+h^2)}\left[\alpha_c + \frac{\alpha_h}{2}p_\perp(\theta)\right] + \frac{\omega^2}{\omega_A^2}\Phi$$
$$= \frac{\alpha_h}{2}\frac{D(\theta)p_\perp(\theta)}{(1+h^2)^{1/2}}\frac{\left\langle \Phi D/\left(1+h^2\right)^{1/2}\right\rangle_*}{\alpha_h\left\langle p_\perp\right\rangle_*/2q^2} - \frac{\alpha_h}{2}\frac{D(\theta)p_\perp(\theta)}{(1+h^2)^{1/2}}\frac{\left\langle \Phi D/\left(1+h^2\right)^{1/2}\right\rangle_*}{\alpha_h\left\langle p_\perp\right\rangle_*/2q^2} \quad (9)$$
$$\times \frac{\langle D\rangle_* - \frac{\alpha_c}{2q^2} - \frac{\alpha_h}{2q^2}\langle p_\perp\rangle_*}{\langle D\rangle_* - \frac{\alpha_c}{2q^2} - \frac{\alpha_h}{2q^2}\langle p_\perp\rangle_*(1-H)}.$$

This equation is of the form

$$\frac{d^2\Phi}{d\theta^2} + G(\Phi;\theta) = 0. \quad (10)$$

We then solve for $\frac{d\Phi}{d\theta}(\theta_0)$:

$$\frac{d\Phi}{d\theta}(\theta_0) = -\int_0^{\theta_0} d\theta G(\Phi;\theta); \quad (11)$$

we have made use of the fact that only even eigenmodes are being considered here, $\frac{d\Phi}{d\theta}(\theta = 0) = 0$.

Now, to make further progress, we assume that the energetic particles are important only over the range $-\theta_0 \leq \theta \leq \theta_0$; this assumption is supported by the fact that the amplitude of the eigenfunction shown in Fig. 3 is small for $\theta \gtrsim \pi$. Then, for $|\theta| > \theta_0$, Eq. (10) is the same as in the conventional MHD problem with outgoing wave boundary conditions. We presume that this part of the problem has been solved, and we treat $\frac{1}{\Phi}\frac{d\Phi}{d\theta}(\theta_0)$ as a known quantity. This term represents the removal of energy off to infinity in the form of shear Alfvén waves and is thus a source of positive dissipation. If $h(\theta) \gg 1$ for $\theta \gtrsim \theta_0$, we would find $\frac{d}{d\theta}\ell n\Phi(\theta_0) = i\omega/\omega_A$. The correct result for finite $h(\theta)$ is considerably different from this, but the imaginary part should still have the same sign,

$$\left(\mathrm{Im}\frac{d}{d\theta}\ell n\Phi\right)\left(\mathrm{Re}\frac{\omega}{\omega_A}\right) > 0,$$

so that the positive dissipation remains.[14]

Furthermore, if we assume $\Phi =$ constant over $0 < \theta < \theta_0$, we obtain

$$\left[\frac{\omega^2}{\omega_A^2} + \frac{1}{\theta_0}\frac{d}{d\theta}\ell n\Phi\left(\theta_0\right) + \gamma_c^2 + \gamma_h^2 - \gamma'^2_h \frac{\left\langle D/\left(1+h^2\right)^{1/2}\right\rangle_*}{\alpha_h \left\langle p_\perp\right\rangle_* /2q^2}\right]$$
$$+ \left\{\gamma'^2_h \frac{\left\langle D/\left(1+h^2\right)^{1/2}\right\rangle_*}{\alpha_h \left\langle p_\perp\right\rangle_* /2q^2}\left[\left\langle D\right\rangle_* - \frac{\alpha_c}{2q^2} - \frac{\alpha_h}{2q^2}\left\langle p_\perp\right\rangle_*\right]\right\} \tag{12}$$
$$\times \left[\left\langle D\right\rangle_* - \frac{\alpha_c}{2q^2} - \frac{\alpha_h}{2q^2}\left\langle p_\perp\right\rangle_*\left(1-H\right)\right]^{-1} = 0,$$

where

$$\gamma_c^2 \equiv \int_0^{\theta_0} \frac{d\theta}{\theta_0}\left\{\frac{\alpha_c D(\theta)}{(1+h^2)} - \frac{1}{(1+h^2)}\left[\frac{(dh/d\theta)^2}{(1+h^2)} + h\frac{d^2h}{d\theta^2}\right]\right\},$$

$$\gamma_h^2 \equiv \int_0^{\theta_0} \frac{d\theta}{\theta_0}\frac{\alpha_h}{2}\frac{p_\perp(\theta)D(\theta)}{(1+h^2)},$$

$$\gamma'^2_h \equiv \int_0^{\theta_0} \frac{d\theta}{\theta_0}\frac{\alpha_h}{2}\frac{p_\perp(\theta)D(\theta)}{(1+h^2)^{1/2}}.$$

This dispersion relation has the form $A(\Omega) + C/B(\Omega) = 0$, or

$$A(\Omega)B(\Omega) + C = 0, \tag{13}$$

with

$$A(\Omega) = \Omega^2 + \frac{1}{\theta_0}\frac{d}{d\theta}\ell n\Phi\left(\theta_0\right) + \gamma_c^2 + \gamma_h^2 - \gamma'^2_h \frac{\left\langle D/\left(1+h^2\right)^{1/2}\right\rangle_*}{\alpha_h \left\langle p_\perp\right\rangle_* /2q^2},$$

$$B(\Omega) = \frac{\left[\left\langle D\right\rangle_* - \frac{\alpha_c}{2q^2} - \frac{\alpha_h}{2q^2}\left\langle p_\perp\right\rangle_*\left(1-H\right)\right]}{\left(\left\langle D\right\rangle_* - \frac{\alpha_c}{2q^2} - \frac{\alpha_h}{2q^2}\left\langle p_\perp\right\rangle_*\right)},$$

$$C = \gamma'^2_h \frac{\left\langle D/\left(1+h^2\right)^{1/2}\right\rangle_*}{\alpha_h \left\langle p_\perp\right\rangle_* /2q^2},$$

and $\Omega = \omega/\omega_A$. In this form Eq. (13) can be analyzed for stability. However, implicit frequency dependence and other parameter dependence is built into the term $\frac{d}{d\theta}\ln\Phi\left(\theta_0\right)$, which this analysis does not evaluate very accurately. However, if we use the numerically found $\frac{d}{d\theta}\ln\Phi\left(\theta_0\right)$, we find that Eq. (13) accurately predicts the numerical eigenvalues.[21]

To proceed with further analysis requires that C be considered as a small parameter, an assumption that is not truly justified at parameters for α_h and α_c near marginal stability.

Nonetheless, making this assumption allows us to see the relation of Eq. (13) in the tokamak case, with the results of similar theory in mirror geometry.[11,31] The assumption that C is small becomes valid as α_h is increased. We now choose Ω_1 and Ω_2 so that $\mathrm{Re}\,A(\Omega_1) \equiv A_R(\Omega_1) = 0$ and $\mathrm{Re}\,B(\Omega_2) \equiv B_R(\Omega_2) = 0$. We also assume that Ω_1, Ω_2 are real and nearly equal to each other, and that $\mathrm{Im}\,A \equiv A_I$, $\mathrm{Im}\,B \equiv B_I$, C are typically small in comparison with A_R and B_R. This type of procedure has also been used in a similar problem in mirror machines by Wong et al.[32] Then, we can write the full solution to Eq. (13) as $\Omega = \Omega_1 + \delta\Omega_1 = \Omega_2 + \delta\Omega_2$, with $\delta\Omega_1$, $\delta\Omega_2 \ll \Omega$. Expanding A and B about Ω_1 and Ω_2, respectively, Eq. (13) becomes approximately

$$\left[(\Omega-\Omega_1)\frac{\partial A_R}{\partial\Omega}(\Omega_1)+iA_I(\Omega_1)\right]\left[(\Omega-\Omega_2)\frac{\partial B_R}{\partial\Omega}(\Omega_2)+iB_I(\Omega_2)\right]+C=0, \qquad (14)$$

where

$$\frac{\partial A_R}{\partial\Omega}(\Omega_1)\cong 2\Omega_1,$$

$$A_I=\mathrm{Im}\left[\frac{1}{\theta_0}\frac{d}{d\theta}\ell n\Phi(\theta_0)\right],$$

$$\frac{\partial B_R}{\partial\Omega}(\Omega_2)=-\frac{\omega_A}{\omega_{d0}}\frac{\frac{\alpha_h}{2q^2}\langle p_\perp\rangle_*\frac{d}{da}(\mathrm{Re}\,H)}{\left[\langle D\rangle_*-\frac{\alpha_c}{2q^2}-\frac{\alpha_h}{2q^2}\langle p_\perp\rangle_*\right]^2},$$

and

$$B_I(\Omega_2)=\frac{\frac{\alpha_h}{2q^2}\langle p_\perp\rangle_*\,\mathrm{Im}\,H}{\langle D\rangle_*-\frac{\alpha_c}{2q^2}-\frac{\alpha_h}{2q^2}\langle p_\perp\rangle_*}.$$

We have neglected any contribution to $\partial A_R/\partial\Omega$ made by $\frac{d}{d\theta}\ell n\Phi(\theta_0)$. This dispersion relation exhibits the typical form for the interaction of two waves, each with its associated dissipation, providing two damped roots in the limit $C \to 0$ [assuming $A_I/\left(\partial A_R/\partial\Omega\right)$ and $B_I/\left(\partial B_R/\partial\Omega\right)$ are positive, as we will show below].

The normalization we use here is that $\langle\omega_d\rangle_*/\omega_A < 0$ without drift reversal, i.e., when $\langle D\rangle_* - \frac{\alpha_c}{2q^2} - \frac{\alpha_h}{2q^2}\langle p_\perp\rangle_* > 0$. With drift reversal, each of these quantities changes sign, e.g., $\langle\omega_d\rangle_*/\omega_A > 0$. The solution of $B_R(\Omega_2) = 0$ implies that

$$\mathrm{Re}\,H=\frac{-\left[\langle D\rangle_*-\frac{\alpha_c}{2q^2}-\frac{\alpha_h}{2q^2}\langle p_\perp\rangle_*\right]}{\frac{\alpha_h}{2q^2}\langle p_\perp\rangle_*}, \qquad (15a)$$

or

$$\mathrm{Re}\, H - 1 = \frac{-\left[\langle D\rangle_* - \frac{\alpha_c}{2q^2}\right]}{\frac{\alpha_h}{2q^2}\langle p_\perp\rangle_*}. \tag{15b}$$

Solutions to these equations in cases without drift reversal are such that $a > 0$. For instance, near drift reversal, the right-hand side of Eq. (15a) is small and negative; at the same time $|a| = |\omega/\langle\omega_d\rangle_*|$ should be large since $\langle\omega_d\rangle_*$ is near zero. We can then use the asymptotic expansion for $Z\left(a^{1/2}\right)$ to find[30]

$$H(a) \cong -\frac{7}{2a}. \tag{16}$$

Thus,

$$a \cong \frac{2}{7}\frac{\frac{\alpha_h}{2q^2}\langle p_\perp\rangle_*}{\left[\langle D\rangle_* - \frac{\alpha_c}{2q^2} - \frac{\alpha_h}{2q^2}\langle p_\perp\rangle_*\right]},$$

or equivalently

$$\Omega_2 \cong -\frac{\omega_{d0}}{\omega_A}\frac{\alpha_h}{7q^2}\langle p_\perp\rangle_*. \tag{17}$$

Equation (17) then implies that $\Omega_2 < 0$, at least near drift reversal, so $a > 0$ when $\langle\omega_d\rangle_* < 0$, and $a < 0$ if $\langle\omega_d\rangle_* > 0$. Numerical calculations for larger values of $|\langle\omega_d\rangle_*|$ indicate that $a > 0$ in general without drift reversal. However, it is clear from Eq. (15b) that $a \to 0$ as $\langle D\rangle_* - \frac{\alpha_c}{2q^2} \to 0$ since

$$\mathrm{Re}\, H \cong 1 + \frac{2}{5}a \tag{18}$$

for $|a| \ll 1$. Thus, when $\left|\langle D\rangle_* - \frac{\alpha_c}{2q^2}\right| \Big/ \frac{\alpha_h}{2q^2}\langle p_\perp\rangle_* \ll 1$, we find

$$a \cong -\frac{5}{2}\frac{\left[\langle D\rangle_* - \frac{\alpha_c}{2q^2}\right]}{\frac{\alpha_h}{2q^2}\langle p_\perp\rangle_*};$$

so,

$$\Omega_2 \cong \frac{5}{2}\frac{\omega_{d0}}{\omega_A}\frac{\left(\langle D\rangle_* - \frac{\alpha_c}{2q^2}\right)\left(\langle D\rangle_* - \frac{\alpha_c}{2q^2} - \frac{\alpha_h}{2q^2}\langle p_\perp\rangle_*\right)}{\frac{\alpha_h}{2q^2}\langle p_\perp\rangle_*}. \tag{19}$$

Clearly, $\Omega_2 < 0$ and $a < 0$ with drift reversal if $\langle D\rangle_* - \frac{\alpha_c}{2q^2} > 0$. This is just as we find using Eq. (17). However, when $\langle D\rangle_* - \frac{\alpha_c}{2q^2} < 0$, Ω_2 is positive. Since we must in this case have $\langle\omega_d\rangle_* > 0$ (i.e., $\langle D\rangle_* - \frac{\alpha_c}{2q^2} - \frac{\alpha_h}{2q^2}\langle p_\perp\rangle_* < 0$), a is also positive.

When we solve $A_R(\Omega_1) = 0$, only Ω_1^2 is determined if we neglect any contribution made by $\mathrm{Re}\left(\frac{1}{\theta_0}\frac{d}{d\theta}\ell n\Phi\right)$. Since we require $\Omega_1 \simeq \Omega_2$ for our method to be valid, it is necessary to pick the sign of Ω_1 such that $\Omega_1 = sgn(\Omega_2)\,|\Omega_1|$.

Now we can specify the signs of the various quantities in Eq. (14). As long as $D(\theta) > 0$, $C > 0$. Computing a bounce average of $D(\theta)$ implies a weighting along the field line much like that used in calculating $\gamma_h'^2$ where the weighting function is approximately $p_\perp(\theta)$. Thus, $\left\langle D/\left(1+h^2\right)^{1/2}\right\rangle_*$ and $\gamma_h'^2$ should have the same sign in most cases, even if $D(\theta) < 0$ for some distance along the field line. It is then reasonable to assume $C > 0$ in general.

The signs of $\frac{\partial A_R}{\partial\Omega}$ and A_I should follow that of Ω_1, since we expect $\left(\mathrm{Im}\frac{d}{d\theta}\ell n\Phi\right)\left(\mathrm{Re}\frac{\omega}{\omega_A}\right) > 0$. To determine $\frac{\partial B_R}{\partial\Omega}$ we need to know $\frac{d}{da}(\mathrm{Re}\,H)$. From both Eq. (16) and Eq. (18), it appears that $\frac{d}{da}(\mathrm{Re}\,H) > 0$. Numerical calculations for values of a intermediate between those for which Eqs. (16) and (18) are valid indicate that this is always the case. Thus, $\frac{\partial B_R}{\partial\Omega} < 0$ in all instances.

If we note that $\mathrm{Im}\,Z(\zeta) = \sqrt{\pi}\exp(-a^2)$ for ζ real, and $\mathrm{Re}\,Z(\zeta) = 0$ when ζ is purely imaginary,[30]

$$B_I = \begin{cases} \dfrac{\frac{8}{15}\sqrt{\pi}a^{7/2}e^{-a}\frac{\alpha_h}{2q^2}\langle p_\perp\rangle_*}{\langle D\rangle_* - \frac{\alpha_c}{2q^2} - \frac{\alpha_h}{2q^2}\langle p_\perp\rangle_*}, & a > 0 \\ 0, & a < 0. \end{cases}$$

In order for $\mathrm{Im}\,H$ to have the proper sign, the sign of $a^{1/2}$ must be chosen so that[21] $\left(a^{1/2}\right)\Omega_2 > 0$. Since $\Omega_2 < 0$ without drift reversal and $\Omega_2 > 0$ when $\langle D\rangle_* - \frac{\alpha_c}{2q^2} < 0$, both of these cases with $a > 0$ result in $B_I < 0$.

There are then three different regimes to consider. First, we have the case without drift reversal. From the above discussions, $C > 0$; Ω_1, $\Omega_2 < 0$; $\frac{\partial A_R}{\partial\Omega} < 0$, $A_I < 0$, $\frac{\partial B_R}{\partial\Omega} < 0$, and $B_I < 0$ in this regime. From Eq. (14) it can be shown that Ω is real if

$$C = A_I B_I\left[1 + \frac{(\Omega_1 - \Omega_2)^2}{\left(\frac{A_I}{\partial A_R/\partial\Omega} + \frac{B_I}{\partial B_R/\partial\Omega}\right)^2}\right]. \tag{19}$$

Smaller values of C yield stability; that is, in the limit $C \to 0$, $A(\Omega)$ and $B(\Omega)$ decouple, and we get two damped roots [see Eq. (14)]. $\frac{\partial A_R}{\partial\Omega}$ and $\frac{\partial B_R}{\partial\Omega}$ represent, respectively, positive and negative energy waves here (the wave energies are actually related to $\Omega_1\frac{\partial A_R}{\partial\Omega}$ and

$\Omega_2 \frac{\partial B_R}{\partial \Omega}$). Similarly, A_I and B_I correspond to positive and negative dissipation, respectively. The primary destabilization mechanism operating at large α_h is that the negative energy precessional mode is being driven unstable by the positive dissipation while the stabilizing influence of the negative dissipation provides a marginally stable point at a smaller, nonzero value of α_h [e.g., curve (ii) in Fig. 1]. Presumably, Eq. (19) is satisfied at this marginal point.

In the second regime, drift reversal is reached by using the energetic particle diamagnetism; that is, $\langle D \rangle_* - \frac{\alpha_c}{2q^2} - \frac{\alpha_h}{2q^2} \langle p_\perp \rangle_* \lesssim 0$, but $\langle D \rangle_* - \frac{\alpha_c}{2q^2} > 0$. All quantities have the same sign as in the first regime, except $B_I = 0$. Marginal stability is obtained in this case only when $C = 0$. We still have the negative energy precessional mode being destabilized by its interaction with the positive energy wave and the positive dissipation, but the stabilizing influence of the negative dissipation is gone. Thus, we always have instability in this regime as long as there is finite coupling ($C \neq 0$) between A and B. This result is familiar from mirror theory.[32]

Finally, in the third regime, drift reversal is reached without the energetic particle diamagnetism, so that $\langle D \rangle_* - \frac{\alpha_c}{2q^2} < 0$, and consequently $\langle D \rangle_* - \frac{\alpha_c}{2q^2} - \frac{\alpha_h}{2q^2} \langle p_\perp \rangle_* < 0$. As discussed above, the signs of the various terms in Eq. (14) are now: $C > 0$; Ω_1, $\Omega_2 > 0$; $\frac{\partial A_R}{\partial \Omega} > 0$, $A_I > 0$, $\frac{\partial B_R}{\partial \Omega} < 0$, and $B_I < 0$. The system is completely stable in this regime. To see this, consider the "worst case" of $\Omega_1 = \Omega_2$ [e.g., this assumption yields the most stringent requirements on C in Eq. (19)] and $A_I = B_I = 0$ (the uncoupled modes are marginally stable). From Eq. (14) we find

$$\Omega - \Omega_2 = \pm \left[\frac{-C}{(\partial A_R/\partial \Omega)\,(\partial B_R/\partial \Omega)} \right]^{1/2} . \tag{20}$$

Since $\frac{\partial A_R}{\partial \Omega} \frac{\partial B_R}{\partial \Omega} < 0$ in this regime, Ω is real. Note that using $B_I = 0$ is somewhat appropriate since $B_I = 0$ as we cross from the second regime into this one. The most important effect here is that $\Omega_2 \frac{\partial B_R}{\partial \Omega}$ has changed sign relative to what it was in the other two cases while the sign of $\Omega_1 \frac{\partial A_R}{\partial \Omega}$ has remained the same. This indicates that the precessional mode has changed to a positive energy wave; likewise, its associated dissipation (still a stabilizing influence) has also become positive in character. Thus, we now have two positive energy

waves coupled together, and we expect the system to be stable. Again, similar results have been obtained for mirror geometries.[33]

It appears that the sloshing ion distribution must be arranged so that $\langle D \rangle_* - \frac{\alpha_c}{2q^2} < 0$ in order for the precessional mode to be stable. While this may be the case for some range of pitch angles in each of the two sloshing distributions, Eqs. (2) and (3), it is not true for all pitch angles. One important shortcoming of this analytic treatment is that the behavior at only one pitch angle λ_* is accounted for; however, the numerical calculations include contributions from all allowed pitch angles. Some of these contributions may yield instability when subjected to the criteria described here. As is clear from Eq. (4b), the relative weightings of the various pitch angles can be affected by the form of the eigenfunction. The plot of $\delta Q(\theta)$ shown in Fig. 3 indicates an emphasis on pitch angles having turning points near $\theta = 0$. Since these pitch angles would most likely fall into the first regime discussed above, the existence of instability in that case is consistent with these results. If we could remove all of the energetic particles trapped near $\theta = 0$, we might be able to eliminate the precessional mode. However, this implies very low energetic particle pressure at $\theta = 0$ relative to the peak values. If we are to stabilize the MHD ballooning mode, this pressure must be significant.

Part of the problem here is that there is only a very short distance along the field line in which $D(\theta) < 0$; the geodesic curvature contribution ($\sim S\theta \sin\theta$) keeps $D(\theta)$ from vanishing except near $\theta = \pi$ where $\sin\theta = 0$. If $D(\theta)$ included contributions from only the normal curvature, it might be possible to arrange for the fraction of pitch angles in a sloshing ion distribution corresponding to instability to be quite small and still maintain sufficient pressure at $\theta = 0$ to stabilize the MHD ballooning mode. With the geodesic curvature included, sloshing distributions of the type described in Sec. II are such that most of the pitch angles in the system fall into the second regime in which the precessional mode is unstable. Thus, at least as far as the tokamak is concerned, the introduction of sloshing particles only removes a stabilizing influence: the negative dissipation.

We can apply the same procedures employed in obtaining Eq. (9) from Eqs. (4a) and

(4b) to the asymptotic continuum limit given by Eqs. (6a) and (6b) to find

$$\frac{d^2\Phi}{d\theta^2}+\frac{\omega^2}{\omega_A^2}\Phi=\frac{\alpha_h}{2}\frac{\sin\theta\quad p_{\perp,t}(\theta)\left\langle\Phi\sin\theta\right\rangle_* H}{\left\{\left\langle D\right\rangle_*-\frac{\alpha_c}{2q^2}-\frac{\alpha_h}{2q^2}\left[\left\langle p_{\perp,p}\right\rangle_*+\left\langle p_{\perp,t}\right\rangle_*(1-H)\right]\right\}}. \tag{21}$$

We have split $p_\perp(\theta)$ into contributions from trapped ($p_{\perp,t}$) and passing ($p_{\perp,p}$) particles so that $p_\perp = p_{\perp,p}+p_{\perp,t}$. Of course when considering distributions such as Eq. (2), $p_{\perp,p}=0$. Here, we want to examine more closely the $k=1/2$ solution to this equation, found to be unstable with the circulating-trapped distribution Eq. (3).

This instability is primarily a result of having $p_{\perp,p}$, $p_{\perp,t}$, $p_\perp \gg 1$ on the inside edge of the tokamak. Such a high level of anisotropy is necessary in a distribution containing trapped particles with turning points near $\theta = \pi$. Since $a = -\frac{\omega}{\omega_{d0}}\left\langle\lambda\left(D-\frac{\alpha_c}{2q^2}-\frac{\alpha_h}{2q^2}p_\perp\right)\right\rangle_*^{-1}$, we expect $a\ll 1$ and $H(a)\simeq 1$ when $\alpha_h\sim 1$; in effect, $\left|\omega/\left\langle\omega_d\right\rangle_*\right|\ll 1$, as in EBT theory. Were it not for the $\frac{\alpha_h}{2q^2}\left\langle p_{\perp,p}\right\rangle_*$ term in the denominator of Eq. (21), we could analyze these equations in a manner similar to that used in EBT theory where $\left\langle p_{\perp,p}\right\rangle_*=0$.[34]

We can solve Eq. (21) approximately by assuming that $p_{\perp,t}$ consists of delta functions at some angle θ_p,

$$p_{\perp,t}(\theta)\simeq p_t\left[\delta\left(\theta+\theta_p\right)+\delta\left(\theta-\theta_p\right)\right].$$

We choose p_t so that this function has the same average as the one used in the numerical calculations,

$$p_t=\int_0^\pi d\theta p_{\perp,t}(\theta).$$

Integrating Eq. (21) with initial conditions $\Phi(-\pi)=0$, $\frac{d\Phi}{d\theta}(-\pi)=1$, we find

$$\Phi(\theta)=\Phi_0(\theta)+\Lambda\Phi_1(\theta), \tag{22}$$

where

$$\Phi_0(\theta)=\frac{\sin\left[\Omega(\theta+\pi)\right]}{\Omega},$$

$$\Phi_1(\theta)=\frac{p_t\sin\theta_p}{\Omega}\left\{\sin\left[\Omega\left(\theta-\theta_p\right)\right]H_0\left(\theta-\theta_p\right)-\sin\left[\Omega\left(\theta+\theta_p\right)\right]H_0\left(\theta+\theta_p\right)\right\},$$

$$\Lambda=\frac{A\left\langle\Phi_0\sin\theta\right\rangle_*}{1-A\left\langle\Phi_1\sin\theta\right\rangle_*},$$

$$A=\frac{\alpha_h}{2}\frac{H}{\left[\left\langle D\right\rangle_*-\frac{\alpha_c}{2q^2}-\frac{\alpha_h}{2q^2}\left\langle p_{\perp,p}\right\rangle_*-\frac{\alpha_h}{2q^2}\left\langle p_{\perp,t}\right\rangle_*(1-H)\right]},$$

and H_0 is the Heaviside function,

$$H_0(x) = \begin{cases} 0, & x < 0 \\ 1, & x > 0. \end{cases}$$

To obtain a dispersion relation for $k = 1/2$, we need only set $\frac{d\Phi}{d\theta}(\pi) = -1$ (e.g., see Refs. 21 and 22), so that Ω is given by

$$\cos^2 \pi\Omega + \Lambda p_t \sin\theta_p \sin\pi\Omega \sin\Omega\theta_p = 0. \tag{23}$$

In computing a bounce average of some function $f(\theta)$, the value of the function at the turning point θ_T receives heavy weighting due to the $1/|v_\parallel|$ factor. We can then get an estimate for Λ if we approximate $\langle f \rangle_* \simeq f(\theta_T)$. Since $\lambda_* \simeq 1$ for a sloshing distribution, the corresponding turning point is near θ_0. But, $\theta_0 \equiv \pi$ for the case we are considering; so $\theta_T \simeq \theta_0 \equiv \pi$. Likewise, the fact that the pressure function $p_{\perp,t}$ peaks near $\theta = \pi$ implies that we should select $\theta_p \simeq \pi$. We can then reasonably set $\theta_T \simeq \theta_p \simeq \pi$ and $\langle f \rangle_* \simeq f(\theta_p)$ in Eq. (23) to obtain

$$\Omega \cot \pi\Omega = -A p_t \sin^2 \theta_p. \tag{24}$$

As mentioned previously, when $\alpha_h \sim 1$ we can assume $\left|\alpha_h \langle p_{\perp,p} \rangle_*\right| > \left|2q^2 \langle D \rangle_* - \alpha_c\right|$ and $H(a) \simeq 1$. If we look for purely imaginary solutions with $\pi \mathrm{Im}\,\Omega > 1$, we see that

$$\gamma = \mathrm{Im}\,\Omega \cong \left(\frac{\int_0^\pi d\theta p_{\perp,t}(\theta)}{\langle p_{\perp,p} \rangle_*} \right) q^2 \sin^2 \theta_p.$$

For the parameters we have been using here, $\gamma \simeq 0.6$, on the order of MHD growth rates as was found through the numerical calculations.

We now examine the behavior of this mode at small α_h. Recall that in Sec. IV no nonzero threshold α_h was found numerically. It appears from Eq. (24) that a sufficient condition for stability is that $A > 0$. With $H = 1$, this implies that the approximate threshold for α_h would be such that

$$\langle D \rangle_* - \frac{\alpha_c}{2q^2} - \frac{\alpha_h}{2q^2} \langle p_{\perp,p} \rangle_* = 0. \tag{25}$$

Implicit in this result is the assumption that $\Omega \to 0$ at marginal stability. However, with $k = 1/2$ and $\alpha_h = 0$ in Eq. (21), we must have $\Omega = \pm 1/2$. Furthermore, if Eq. (25) is nearly

satisfied, $\langle\omega_d\rangle_*$ should not be very large. As a result, we cannot assume $\omega/\langle\omega_d\rangle_* \ll 1$ and $H = 1$ near marginal stability.

At small α_h, resonant particles arising from the overall drop in the energetic particle diamagnetic contribution to $\langle\omega_d\rangle_*$ provide an imaginary part for the kinetic integral in Eq. (6b). As a result, the shear Alfvén waves near $\Omega = -1/2$ are destabilized at all small, but nonzero, values of α_h. This is the effect shown in Fig. 5.

VI. Conclusions

The numerical calculations carried out here suggest several problems with using energetic sloshing ions to eliminate resonant particle destabilization of ballooning modes. Computations made with a distribution containing only trapped particles point out that the requirement $\tau > 0$ necessary to avoid mirror-mode instability and to prevent numerical problems sets a lower limit on the width of the distribution in pitch angle space. The numerical results in this case indicate that the sloshing ions do not have a strong stabilizing effect on the high-frequency ($\omega \sim \langle\omega_d\rangle$) branch of solutions to the ballooning mode equations. It is also noted that at large energetic particle pressures the boundary conditions of outgoing waves and spatially damped waves at infinity are no longer consistent. Investigations of the ballooning mode equations in the $S\theta \to \infty$ limit point to a continuum instability as the source of this problem. The instability results from the destabilization of shear Alfvén waves by the negative dissipation due to resonant particles in the distribution.

By employing a distribution containing both circulating and trapped energetic particles, the restrictions imposed to keep $\tau > 0$ can be relaxed significantly. In this case, the turning points of the trapped particles can be concentrated on the inside edge of the tokamak sufficiently well to eliminate almost all of the resonant particles so that the continuum solutions are nearly stable. However, another branch of continuum solutions is predicted to be unstable as a result of the presence of a large energetic particle pressure peak in the good curvature region. This instability has been examined analytically and found to have a growth rate on the order of MHD time scales. Furthermore, it is unstable for all nonzero values of the energetic particle pressure gradient. Thus, it appears that at least one of the two branches of the continuum solutions is always unstable for a sloshing distribution

in the high-bounce-frequency regime. As long as this is true, an unstable solution can be found to the ballooning mode equations.

Analytic calculations examining the high-frequency, precessional mode show that changing the sign of $\langle\omega_d\rangle$ (i.e., so that $\omega_* \langle\omega_d\rangle < 0$) through diamagnetic effects does not provide stability since doing so removes the one stabilizing influence in the system: the negative dissipation arising out of the drift resonance. The stabilizing effect of the sloshing particles appears only if $\omega_* \langle\omega_d\rangle < 0$ when the energetic particle diamagnetic contribution to $\langle\omega_d\rangle$ is not included. In the tokamak geometry this is a much more stringent condition than in a simple mirror due to the presence of the (unfavorable) geodesic curvature in $\langle\omega_d\rangle$. Attempts to satisfy it would most likely lead to destabilization of the MHD ballooning branch or would fail as a result of the eigenfunction peaking in such a way that the effects of remnant unstable particles in the system are heavily weighted.

These several problems: the limitations imposed to keep $\tau > 0$, the continuum instabilities, and the difficulty of achieving $\omega_* \langle\omega_d\rangle < 0$ without the energetic particle diamagnetic contribution, in addition to the larger volume of hot plasma required for a sloshing distribution, lead us to conclude that sloshing energetic particles would be less effective in bridging the unstable gap to second stability than a deeply-trapped distribution of the same energy.

Acknowledgements

The authors wish to acknowledge fruitful discussions with M. N. Rosenbluth and J. W. Van Dam. This research was supported by U. S. Department of Energy Contract #DE-FG05-80ET-53088.

References

1. J. W. Connor, R. J. Hastie, T. J. Martin, and M. F. Turner, *Proceedings of the Third Joint Varenna–Grenoble International Symposium on Heating in Toroidal Plasmas* (Comm. of the European Communities, Brussels, 1982), Vol. 1, p. 65.
2. R. J. Hastie and K. W. Hesketh, Nucl. Fusion **21**, 651 (1981).
3. M. N. Rosenbluth, S. T. Tsai, J. W. Van Dam, and M. G. Engquist, Phys. Rev. Lett. **51**, 1967 (1983).
4. D. A. Spong, D. J. Sigmar, W. A. Cooper, D. E. Hastings, and K. T. Tsang, Phys. Fluids **28**, 2494 (1984).
5. G. Rewoldt and W. M. Tang, Nucl. Fusion **24**, 1573 (1984).
6. R. A. Dandl, et al., *Plasma Physics and Controlled Nuclear Fusion Research* (IAEA, Vienna, 1975), Vol. II, p. 141.
7. N. A. Krall, Phys. Fluids **9**, 820 (1966).
8. R. R. Dominguez and H. L. Berk, Phys. Fluids **21**, 827 (1978).
9. J. M. Greene and M. S. Chance, Nucl. Fusion **21**, 453 (1981).
10. M. N. Rosenbluth, J. W. Van Dam, and Y. C. Lee, Phys. Fluids **25**, 1349 (1982).
11. D. E. Baldwin and H. L. Berk, Phys. Fluids **26**, 3595 (1983).
12. K. McGuire, et al., Phys. Rev. Lett. **50**, 891 (1983).
13. L. Chen, R. B. White, and M. N. Rosenbluth, Phys. Rev. Lett. **52**, 1122 (1984).
14. J. Weiland and L. Chen, Phys. Fluids **28**, 1359 (1985).
15. K. McGuire, D. Buchenauer, R. Izzo, J. Manickam, D. Monticello, K. Okano, W. Park, and N. Sauthoff, Bull. Am. Phys. Soc. **28**, 1173 (1983).
16. D. M. Kruskal and C. Oberman, Phys. Fluids **1**, 275 (1958).
17. T. M. Antonsen and Y. C. Lee, Phys. Fluids **25**, 132 (1982).
18. P. J. Catto, R. J. Hastie, and J. W. Connor, Plasma Phys. Controlled Fusion **27**, 307 (1985).
19. M. N. Rosenbluth, Phys. Fluids **11**, 869 (1968).
20. E. L. Ince, **Ordinary Differential Equations** (Dover, New York, 1944).
21. D. P. Stotler, Ph.D. thesis, The University of Texas at Austin, 1986.
22. D. P. Stotler and H. L. Berk, Institute for Fusion Studies Report, IFSR-248 (1986).

23. H. Grad, Phys. Fluids **10**, 137 (1967).

24. R. J. Hawryluk, et al., Phys. Rev. Lett. **49**, 326 (1982).

25. C. Z. Cheng, L. Chen, and M. S. Chance, Ann. Phys. **161**, 21 (1984).

26. J. W. Van Dam and M. N. Rosenbluth, Sherwood Theory Meeting, Madison, Wisconsin, 1985, Paper 1C-6.

27. A. Bers, **Handbook of Plasma Physics**, Chapter 3.2, eds. M. N. Rosenbluth and R. Z. Sagdeev (North-Holland Publishing Company, New York, 1983).

28. H. L. Berk, J. W. Van Dam, M. N. Rosenbluth, and D. A. Spong, Phys. Fluids **26**, 201 (1983).

29. D. P. Stotler, H. L. Berk, and M. G. Engquist, Phys. Fluids **29**, 1149 (1986).

30. B. D. Fried and S. D. Conte, **The Plasma Dispersion Function** (Academic, New York, 1961).

31. H. L. Berk and Y. Z. Zhang, Institute for Fusion Studies Report, IFSR-199 (1985).

32. H. V. Wong, H. L. Berk, and K. T. Tsang, Bull. Am. Phys. Soc. **30**, 1370 (1985).

33. H. L. Berk, M. N. Rosenbluth, H. V. Wong, and T. M. Antonsen, Phys. Fluids **27**, 2705 (1984).

34. H. L. Berk, C. Z. Cheng, M. N. Rosenbluth, and J. W. Van Dam, Phys. Fluids **26**, 2642 (1983).

Figure Captions

1. The imaginary part of the eigenvalue plotted as a function of α_h for $\alpha_c = 0.8$, $\omega_{d0}/\omega_A = .636$, $\Delta\lambda = 10^6$, $\theta_0 = 0.785$, $\omega_{*0} = 0$ in curves (i) and (ii). For curves (iii) and (iv), $\Delta\lambda = 0.02$, and $\theta_0 = 3.04$, with $\omega_{*0} = 0$ for (iii), $\omega_{*0}/\omega_{d0} = 1.10$ for (iv).
2. Marginally stable ($\mathrm{Im}\,\omega/\omega_A = 10^{-3}$) values of α_h for low-frequency, MHD (small α_h) and high-frequency, precessional (large α_h) branches as ω_{d0}/ω_A is varied, with $\alpha_c = 0.8$, $\theta_0 = .785$, $\omega_{*0} = 0$, $\Delta\lambda = 10^6$.
3. Plot of $\mathrm{Re}\delta Q$ (normalized to its value at $\theta = 0$) as a function of θ. Parameters used here are $\alpha_h = 1.88$, $\Delta\lambda = 0.02$, $\theta_0 = 3.04$, and $\omega_{*0}/\omega_{d0} = 1.10$.
4. Plot of $\gamma_{\max}$ as a function of $\log\Delta\lambda$ for the $k = 0$ mode with $\alpha_h = 1.5$, $\omega_{*0} = 0$, $\omega_{d0}/\omega_A = .636$ using: (i) the purely-trapped distribution, Eq. (2) with $\theta_0 = 3.04$, and (ii) the trapped and circulating distribution, Eq. (3).
5. Plot of $\gamma_{\max}$ (i) and the negative of the real part of the frequency (ii) as a function of α_h for the $k = 1/2$ mode using the circulating and trapped distribution, Eq. (3), with $\Delta\lambda = 0.02$, $\omega_{d0}/\omega_A = 5$, $\alpha_c = 0$, $\omega_{*0} = 0$.

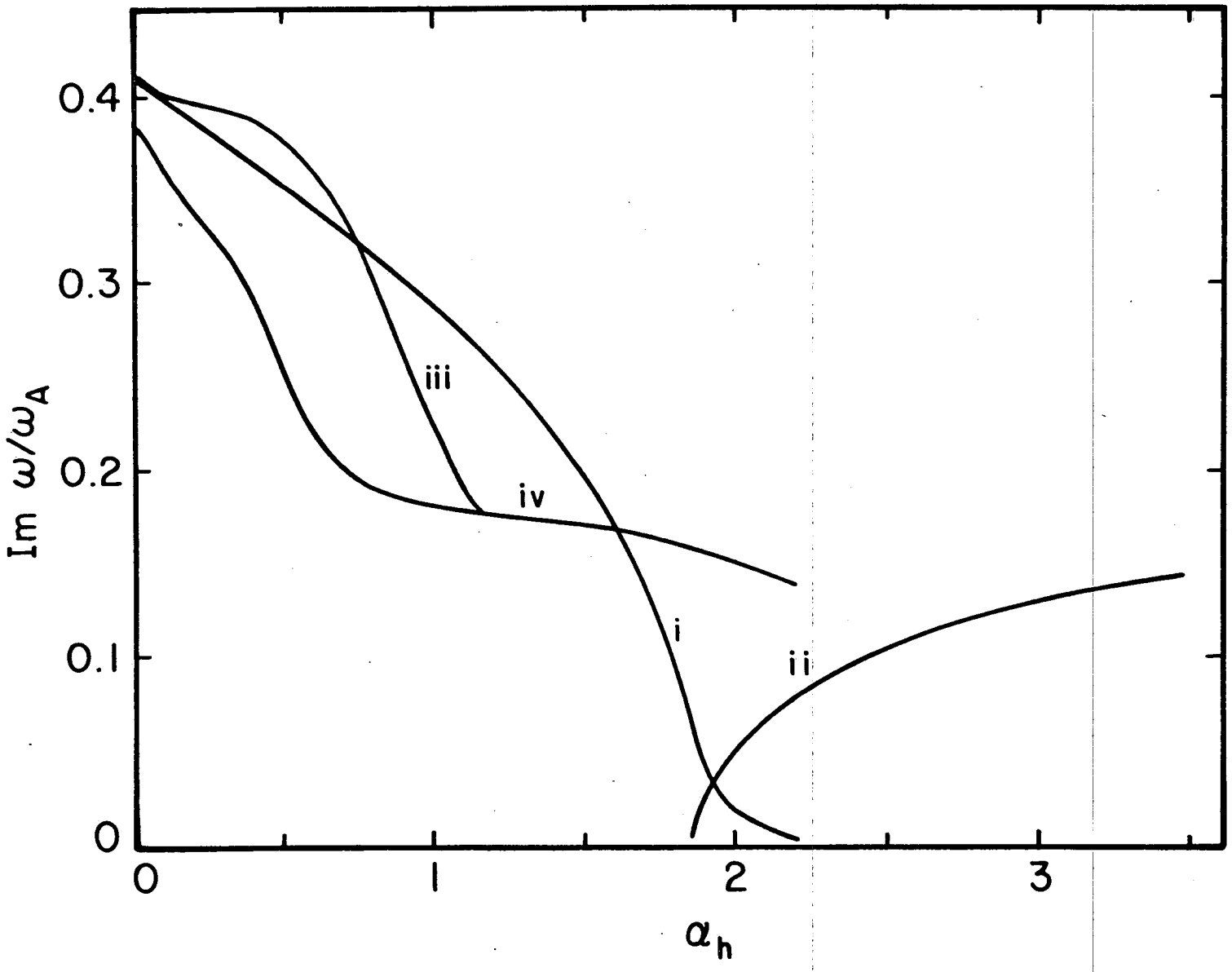

Fig. 1

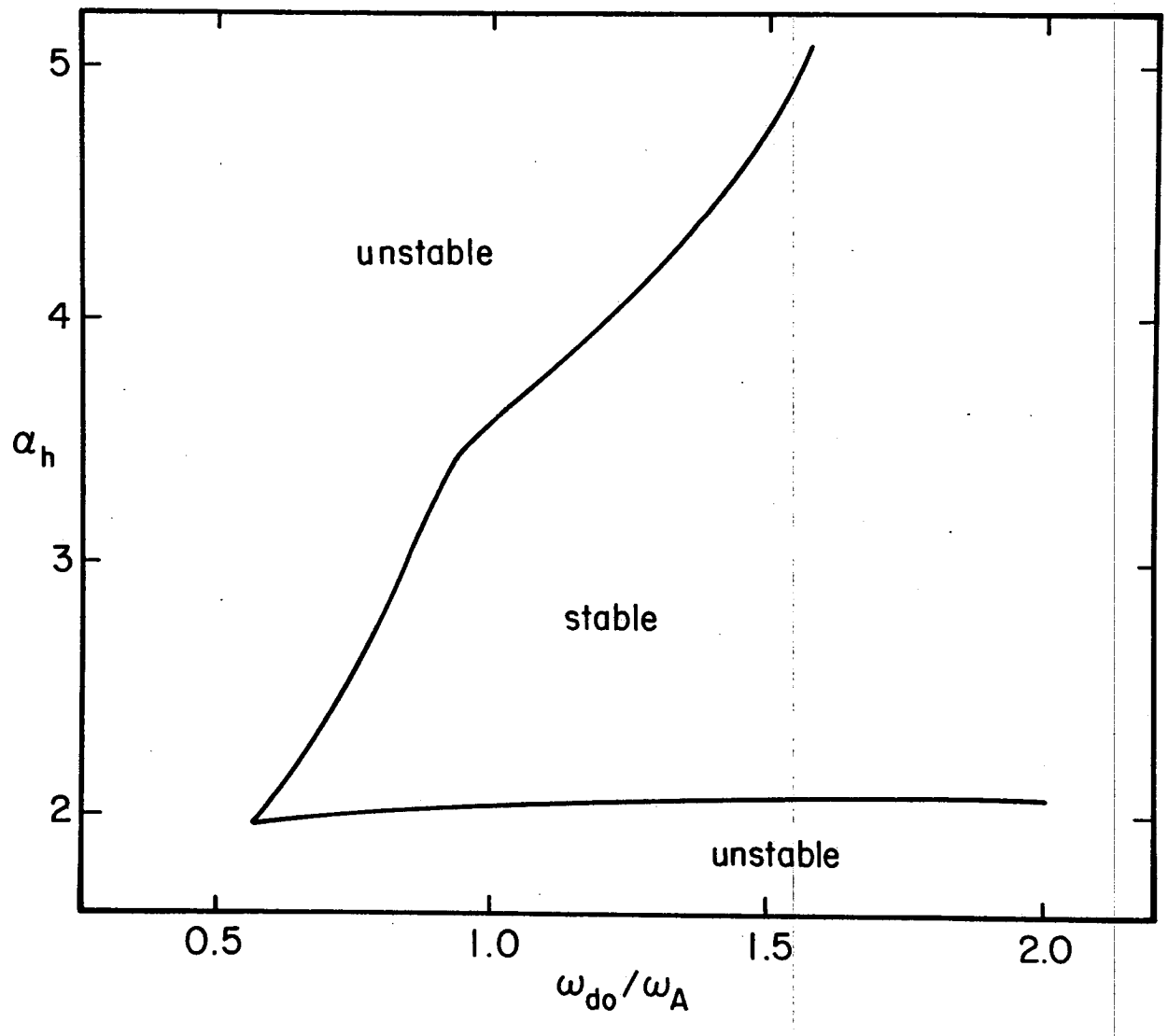
5
4
3
2
α_h
unstable
stable
unstable
0.5
1.0
1.5
2.0
ω_{do}/ω_A

Fig. 2

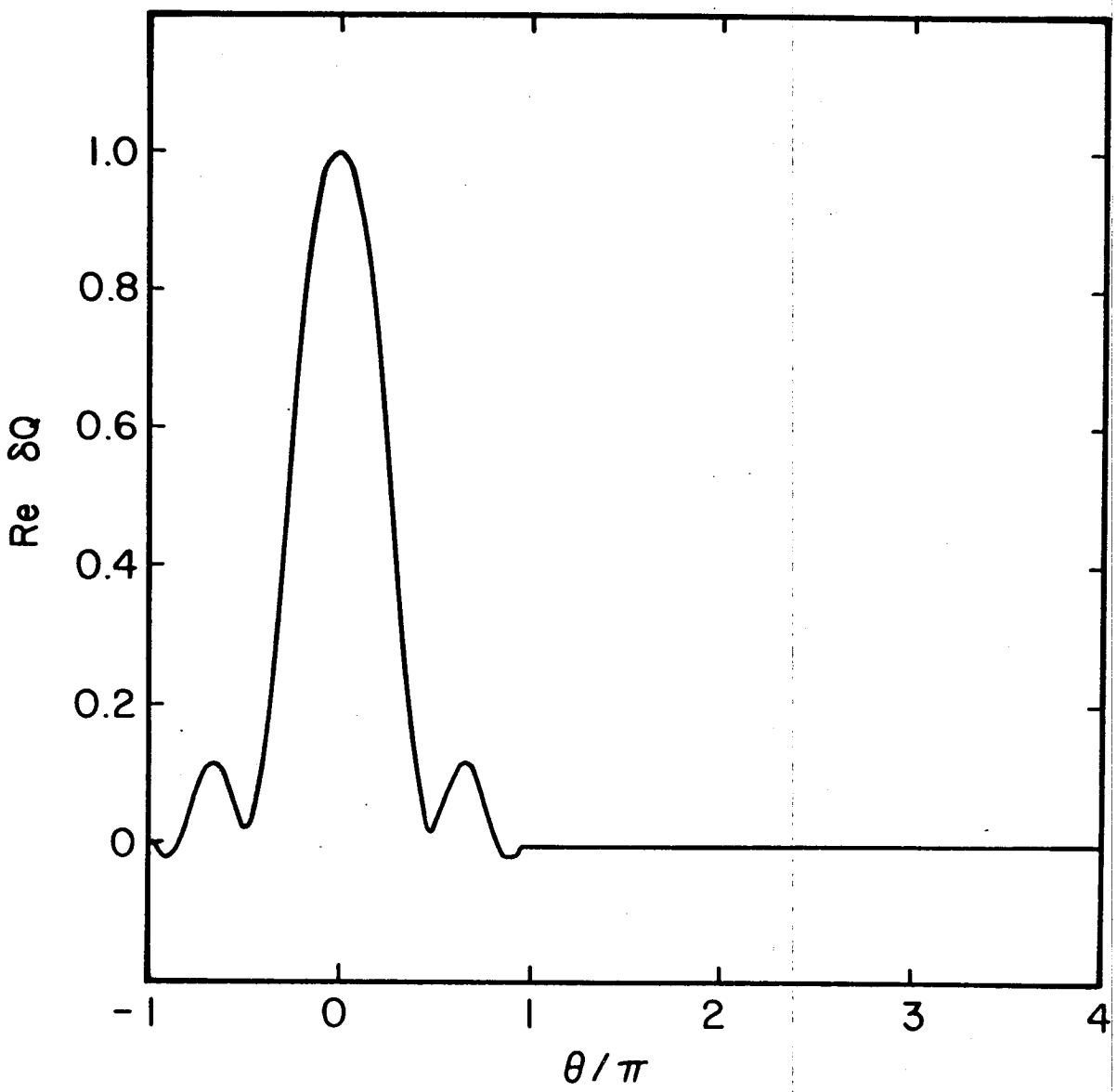

Fig. 3

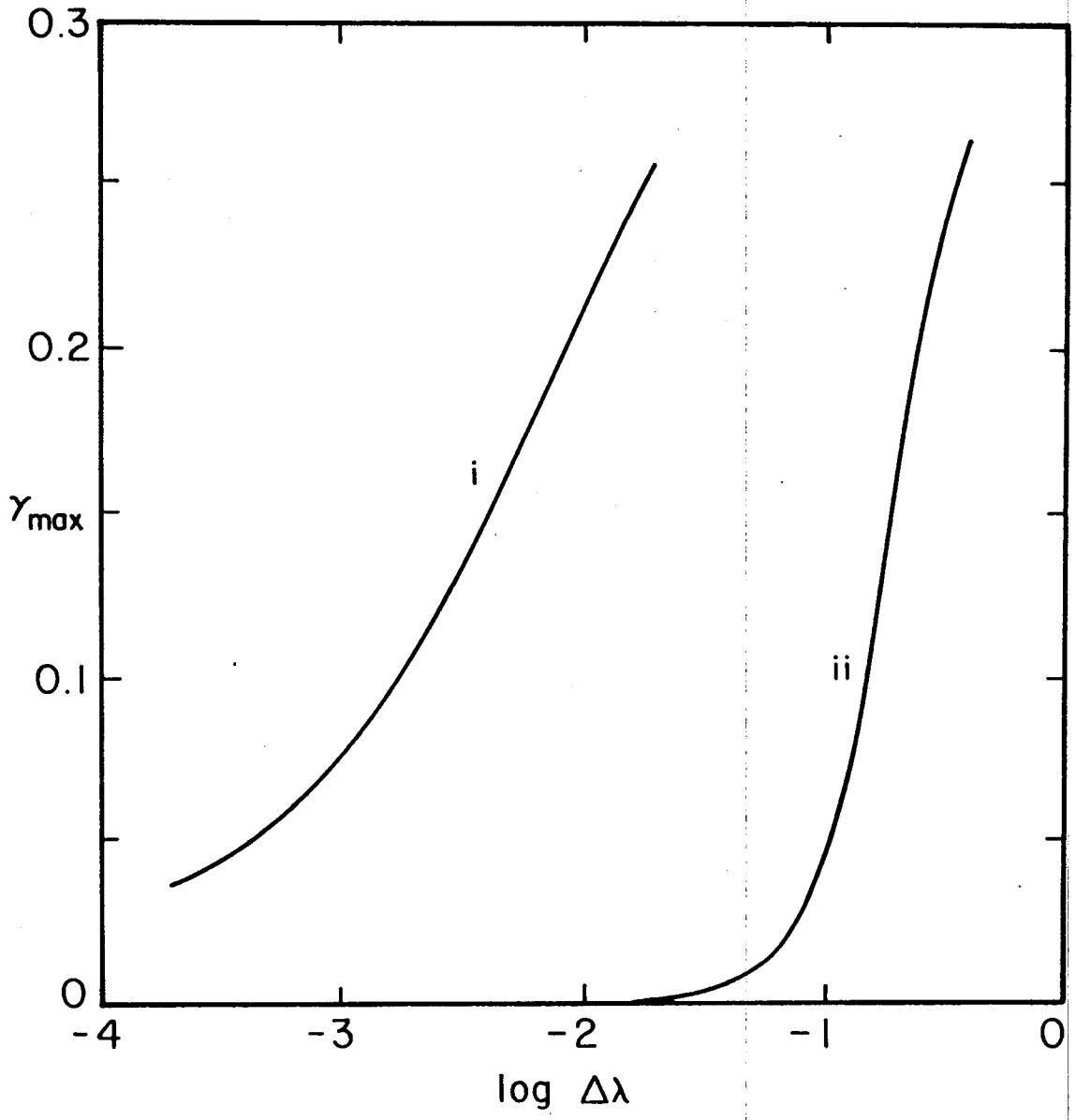

Fig. 4

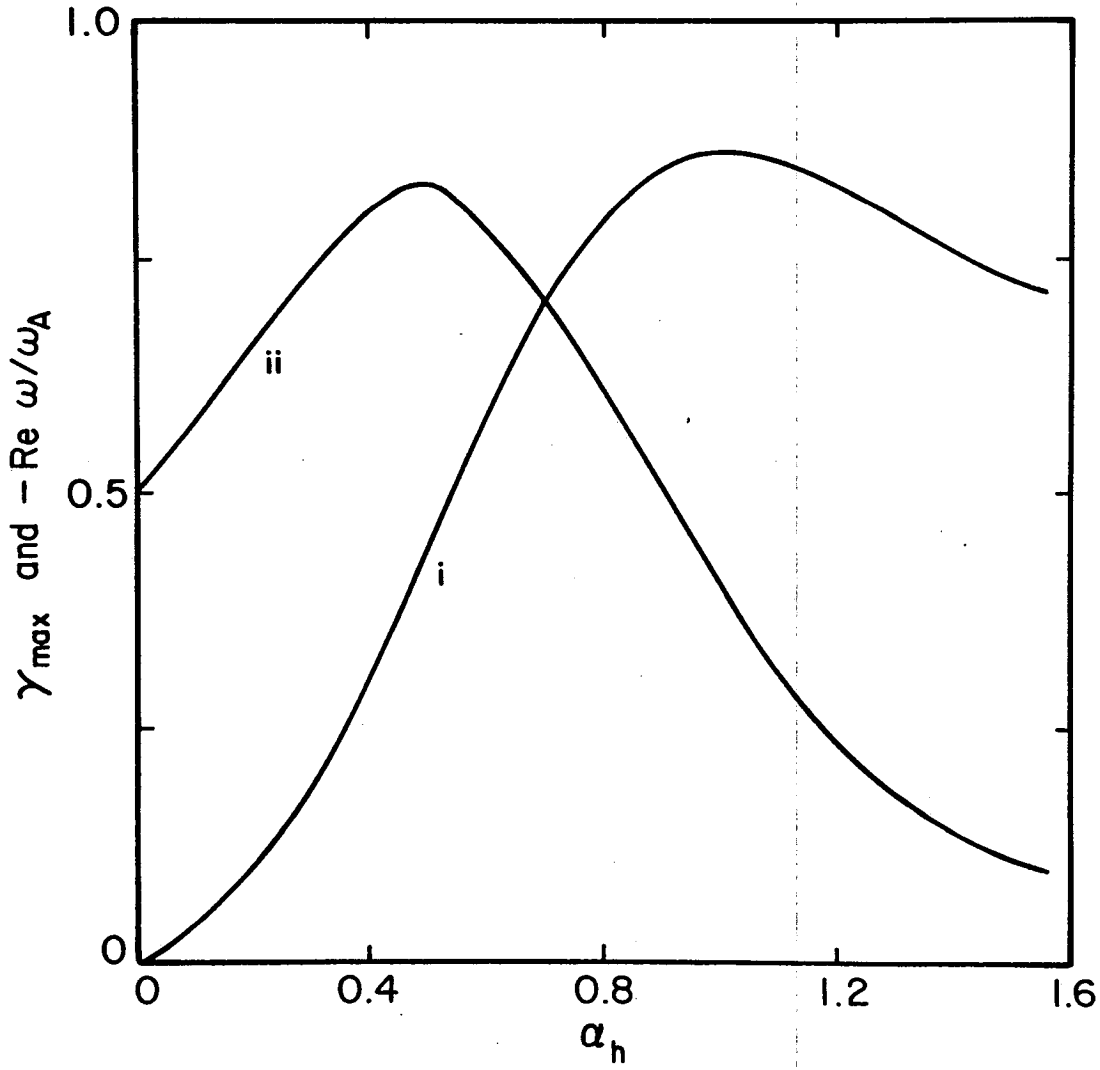

Fig. 5

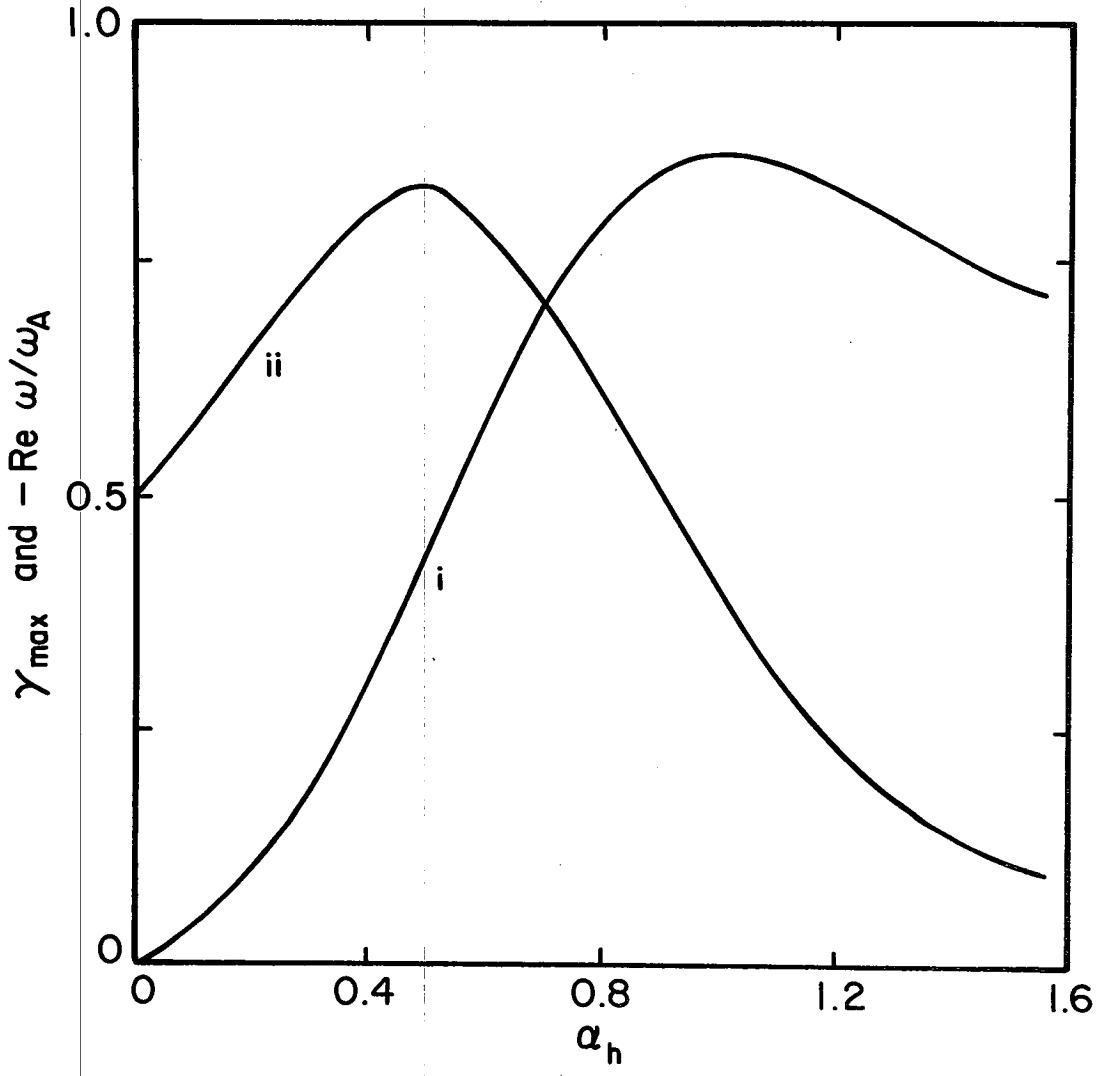
1.0
0.5
0
0
0.4
0.8
1.2
1.6
α_h
γ_{max} and $-$Re ω/ω_A
i
ii